

# Interference Peak in the Spectrum of Bremsstrahlung on Two Amorphous Targets

M.V. Bondarenco\* and N.F. Shul'ga

*NSC Kharkov Institute of Physics and Technology, 1 Academic St., 61108 Kharkov, Ukraine*

(Dated: June 29, 2021)

We investigate the interference pattern in the spectrum of non-dipole bremsstrahlung on two amorphous foils. Apart from suppression at lowest  $\omega$ , the spectrum exhibits an enhancement adjacent to it. In classical electrodynamics, the net effect of suppression and enhancement proves to be zero. We study the location and the origin of the spectral features, comparing predictions of full Molière averaging with those of the Gaussian averaging with Coulomb corrections to the rms multiple scattering angle. Comparison with experimental data, and with previous theoretical predictions is presented.

PACS numbers: 41.60.-m., 78.80.-g

## I. INTRODUCTION

Suppression of the low-energy part of bremsstrahlung from ultrarelativistic electrons passing through an amorphous scattering medium is the celebrated LPM-effect [1], named after Landau and Pomeranchuk who predicted it qualitatively [2], and Migdal [3] who provided an accurate theory for bremsstrahlung in a semi-infinite uniform medium. It has also been studied for finite-thickness targets [4–8], and for the opposite limit of thin target, which is of intrinsic interest [4, 9]. The theoretical predictions were accurately tested experimentally only within the last two decades [10], and the theoretical and experimental state of the art is reviewed in [11–13].

A natural further step, both for practice and for theory, is to study composite targets. One of the simplest configurations thereof is a sequence of thin plates with a gap between them comparable to the photon formation length

$$l_f = \frac{2E_e}{m_e^2} \left( \frac{E_e}{\omega} - 1 \right). \quad (1)$$

The latter quantity depends on the electron energy  $E_e$  and photon energy  $\omega$  in the window covered by the detector,  $m_e$  standing for the electron mass. The problem of structured target as applied to the gamma-quantum emission, was first discussed by Blankenbecler [14, 15], who treated it at the basis of the model for multiple scattering devised in [6]. Subsequently, other authors [7, 16] extended their formalisms to handle this problem.

An experimental verification of the existence of interference effects in bremsstrahlung on compound targets has recently been undertaken at CERN [17–19]. It was emphasized [18, 19] that high electron energy allows achieving macroscopic values for the photon formation length (1), and thereby study its manifestations simply by tuning the distance between the scattering plates by a micrometer screw. But even for CERN energies,

$E_e \approx 178$  GeV, the coefficient in Eq. (1) amounts only  $\frac{2E_e}{m_e^2} \approx 0.4 \mu\text{m}$ , wherefore to make  $l_f$  practically macroscopic ( $\gtrsim 10^{-2}$  mm), one needs to consider sufficiently small photon energies compared to  $E_e$ , which then renders the problem essentially classical. At the same time, condition  $\omega/E_e \gg 10^{-4}$  can be safely fulfilled, where-with the contribution from transition radiation may be neglected. The experiment [19] conducted at such conditions favored the theory [14], but also found some departures from it, and, surprisingly, from other theoretical predictions, which were expected to be more accurate.

To clarify the origin of remaining discrepancies, it may be instructive to recollect underlying assumptions for the theories at the market. It is fair to say that Blankenbecler and Drell [6] in essence extended Landau and Pomeranchuk's approach [2] to cover the case of finite-thickness target, and incorporate quantum effects. At that, a simplified model of scattering in a medium was adopted, in which transverse dimensions of the target random field exceeded that of the electron wave packet, allowing to exactly integrate over electron impact parameters and to reduce the photon emission amplitude to an integral over particle trajectory, like in classical mechanics. A strong simplification was made then, in the spirit of [2], by replacing the medium average of an oscillatory integrand by the corresponding oscillatory function of averaged variables. That yielded the angle-integral spectrum in the form of a double time integral, which for most cases of interest had to be computed numerically. Along these lines, Blankenbecler [14] evaluated the spectrum of radiation on  $N$  plates, and discovered an additional maximum, or “shoulder” in the region where the gap width becomes commensurable with the radiation coherence length.

The approach of Blankenbecler and Drell has the merit of being simple and qualitatively correct. However, it suffers from a lack of accuracy due to the oversimplified averaging (the neglect of fluctuations), which may be essential for comparison with experiments. An attempt to improve it was undertaken in Blankenbecler's later paper [15], where a correlation of the amplitude and the phase of the integrand in the double time integral was taken into account, while other fluctuations were neglected, as before. As we will show, however, the correction so eval-

---

\*Electronic address: bon@kipt.kharkov.ua

uated improves the accuracy only for the case of weak scattering in the plates, whilst in the opposite case of strong (non-dipole) scattering, in which interference effects are actually the strongest, this correction is rather counterproductive.

Almost simultaneously with [6, 14], Zakharov [7] advanced with a calculation of the LPM effect in finite targets including proper averaging. It was built upon techniques originally developed for particle physics, notably the impact parameter representation. The merit of the latter is that it naturally invokes Fourier transforms of scattering-angle distribution functions, which from solution of the kinetic equation express as simple exponentials of the Fourier-transformed scattering differential cross-section. The main attention in papers [7] was payed to a single finite-thickness target, while for structured target, the results were presented only graphically. Zakharov noticed that the interference features in his calculated spectrum were less pronounced than those in [14], albeit attributed that to the crudeness of the Blankenbecler-Drell model for scattering medium, rather than to an oversimplification of their averaging procedure.

Shortly after, Baier and Katkov [16] proposed a technique which allowed them to handle the case of  $N$  scattering plates analytically. To this end, an alternative form of the double time integral representation for the radiation spectrum was adopted, and radiation spectra for  $N$  plates were calculated by mathematical induction, assuming all the plates to be identical, equidistant, and the scattering angle distributions in them to be Gaussian. The influence of the transition radiation was taken into account too, which can be valuable for lower-energy experiments. Baier and Katkov ultimately restricted their analysis to the case of plates infinitesimally thin compared to the gap width, and demonstrated that instead of one maximum, the radiation spectrum features a sequence of maxima and minima of decreasing amplitude.

The common drawback shared by all the abovementioned approaches is that the resulting expressions for the radiation spectrum are rather unwieldy, and relations of the spectral features with physical parameters in the problem remain obscure. What is more serious, however, is that it led to a number of qualitative controversies in the literature, the most noticeable among which are the following:

- It was suggested in [14] that the position of the greatest spectral maximum corresponds to a situation when the photon formation length (1) matches the distance between the plate centres. But in that case, the resonance condition ought to involve an additional factor  $2\pi$ , as in coherent bremsstrahlung (see [19, 20]). However, therewith it would definitely contradict the experiment [19].
- In the integral expressing the radiation spectrum, the oscillating function typically has the argument  $\frac{\omega t}{2\gamma^2}(1 + \gamma^2\theta^2)$ , where  $\gamma$  is the electron's Lorentz

factor, and  $\theta$  the radiation angle. The use of the latter expression suggests that for the distance  $l_g + l$  between the plate centers, the main spectral maximum should be located at

$$\omega \simeq 2\pi \frac{2\gamma^2}{(l_g + l)(1 + \gamma^2\theta^2)},$$

involving factor  $2\pi$ , as expected, but also a denominator  $1 + \gamma^2\theta^2$ , which might compensate it. Practically, though, it is not a priori obvious, with respect to which direction the radiation angles should be counted, and what are their typical values. If one estimates them as  $\theta \sim \max\{\gamma^{-1}, \sigma\}$ , where  $\sigma$  is the rms scattering angle in the plates [16], then for  $\sigma \gg \gamma^{-1}$  the compensation between the  $2\pi$  factor and the denominator can be significant. But numerically, such estimates still contradict the experimental findings [19].

- Concerning the comparative strength of the contributions from the enhancement region and the suppression region at low  $\omega$ , it is unobvious whether their integrated effect must be zero, as suggested in [22], or the suppression must dominate in the total energy losses, as one might anticipate from the Migdal's theory [3] of radiation in a thick target, where no enhancement manifests itself in the spectrum at all.

In the absence of cogent explanation for those controversies, the state of the theory can hardly be regarded as satisfactory. Besides that, it is becoming desirable further to consider the case of plates of unequal thickness, and to fully scrutinize the role of non-Gaussian (Coulomb) tails in scattering, insofar as approaches of Baier and Katkov, as well as Blankenbecler and Drell rested on Gaussian description of scattering.

Given rather fundamental significance of the present problem, it makes sense at present to reappraise its theoretical treatment. In this paper we shall derive physically more transparent representations for the radiation spectrum, which will help clarify the matter as a whole, and at the same time improve the numerical accuracy. To simplify the problem, we will consider the case of two *thin* scattering plates (foils), which allows avoiding double time integral representations for the radiation spectrum. We will also limit ourselves to classical electrodynamics, and neglect the transition radiation, which are good approximations for the performed experiments [17–19]. On the other hand, we will investigate in more detail the influence of Coulomb corrections. To alleviate the connection between the theory and the experiment, we introduce appropriate visibilities of the interference pattern. We will be able to resolve the controversies alluded above, and to correct abundant numerical errors existing in the literature. Ultimately, we compare our predictions with the recent experimental data, and show that there is no significant discrepancy between the experiment and the theory.

## II. SPECTRUM OF RADIATION AT TWO SCATTERINGS

In classical electrodynamics, the spectral-angular energy distribution of radiation (with vector  $\mathbf{n}$  marking the direction of photon emission) expresses in a known way through the charged particle trajectory  $\mathbf{r}(t)$ ,  $\mathbf{v}(t) = d\mathbf{r}/dt$  [21]:

$$\frac{dI}{d\omega d^2n} = \left| \frac{e}{2\pi} \int_{-\infty}^{\infty} dt e^{i\omega[t - \mathbf{n} \cdot \mathbf{r}(t)]} \frac{d}{dt} \frac{\mathbf{n} \times \mathbf{v}(t)}{1 - \mathbf{n} \cdot \mathbf{v}(t)} \right|^2, \quad (2)$$

$e$  being the electron charge. For our present study, it will suffice to consider the simplest case when the electron experiences 2 abrupt scatterings, at instants  $t_1$  and  $t_2$ :

$$\mathbf{v}_1 \xrightarrow{t_1} \mathbf{v}_2 \xrightarrow{t_2} \mathbf{v}_3.$$

Integration over the time in Eq. (2) trivially yields

$$\frac{dI}{d\omega d^2n} = \left( \frac{e}{2\pi} \right)^2 \left| \mathbf{n} \times \mathbf{J}_{21} + \mathbf{n} \times \mathbf{J}_{32} e^{i\Psi} \right|^2 \quad (3a)$$

$$= \left( \frac{e}{2\pi} \right)^2 \left[ (\mathbf{n} \times \mathbf{J}_{21})^2 + (\mathbf{n} \times \mathbf{J}_{32})^2 + 2(\mathbf{n} \times \mathbf{J}_{21}) \cdot (\mathbf{n} \times \mathbf{J}_{32}) \cos \Psi \right], \quad (3b)$$

with

$$\mathbf{J}_{21}(\mathbf{n}) = \frac{\mathbf{v}_1}{1 - \mathbf{n} \cdot \mathbf{v}_1} - \frac{\mathbf{v}_2}{1 - \mathbf{n} \cdot \mathbf{v}_2}, \quad (4)$$

$$\mathbf{J}_{32}(\mathbf{n}) = \frac{\mathbf{v}_2}{1 - \mathbf{n} \cdot \mathbf{v}_2} - \frac{\mathbf{v}_3}{1 - \mathbf{n} \cdot \mathbf{v}_3}, \quad (5)$$

$$\Psi(\omega, \mathbf{n}) = \omega(t_2 - t_1)(1 - \mathbf{n} \cdot \mathbf{v}_2). \quad (6)$$

Eq. (3a) implies that if scatterings are well separated, the spectral radiation amplitude can be viewed as a sum of spectral amplitudes of radiation at single scatterings (with a distance- and  $\omega$ -dependent phase shift  $\Psi$  between them). That may be conceived as the absence of effects of temporarily nonequilibrium proper field on the radiation amplitude level. However, observed in practice is the radiation intensity, which is proportional to the amplitude square. It differs from a sum of intensities on separate plates, engaging certain dependence on  $\omega$  through the cosine of the phase shift between the scatterings.

An important generic property of Eq. (3b) is that the  $\omega$ -integral of the interference term therein strictly vanishes:

$$\int_0^{\infty} d\omega \left( \frac{dI}{d\omega} - \frac{dI_1}{d\omega} - \frac{dI_2}{d\omega} \right) = 0,$$

by virtue of the relation

$$\int_0^{\infty} d\omega \cos \Psi = \pi \delta [t_{21}(1 - \mathbf{n} \cdot \mathbf{v}_2)], \quad (7)$$

and strictly non-zero value of the argument of the  $\delta$ -function for  $t_{21} = t_2 - t_1 \neq 0$ . The absence of interference in the total radiative energy loss at successive random scatterings has a simple physical reason: Equivalently, it can be expressed as a *time* integral of the particle acceleration squared, in which time-separated scatterings obviously give non-interfering contributions [22]:

$$\int_{-\infty}^{\infty} dt \frac{dI}{dt} = \sum_k \int_{-\infty}^{\infty} dt \frac{dI_k}{dt}.$$

Hence, if a suppression occurs in one region of the spectrum (typically at lowest  $\omega$  where it is associated with the LPM effect), it should be accompanied by a commensurable *enhancement* in some other region (which is natural to call the anti-LPM effect).

The established property is undoubtedly general and must hold as well for a number of scatterings greater than 2. But it may contradict our experience that in a target with  $\delta$ -correlated scatterings, interference effects to the spectrum are purely suppressive, and there is seemingly no enhancement region at all [3]. The contradiction is resolved if one takes into account that in condensed matter, distances between atoms are very short indeed, being usually far shorter than photon formation length. Specifically, if we consider inequality

$$a_B = \frac{1}{m_e e^2} \ll l_f \approx \frac{2E_e}{m_e^2} \frac{E_e}{\omega}, \quad (8)$$

where *quantum* arguments stipulate that  $E_e/\omega > 1$ , condition (8) is fulfilled already at  $E_e \gtrsim \frac{m_e}{e^2} \sim 10^2$  MeV. In the latter (quite ubiquitous) case, the radiation spectrum reaches its quantum end at  $\omega = E_e$  sooner than the radiation enhancement can develop. Therefore, the spectral enhancement has no room to develop, and the suppression dominates both locally and globally [22].

One could imagine that for gaseous targets, where distances between atoms are much greater than  $a_B$ , the situation might change, but in the latter case, it is essential that  $t_{21}$  should be regarded as a random variable. We will return to effects of randomization of  $t_{21}$  in Sec. VIII, and demonstrate that the anti-LPM effect still manifests itself on a scale of photon formation length comparable with the range of *anti*-correlation, which is of order of atomic size, again. Meanwhile, we will concentrate on studying the case of radiation on two scattering foils with definite and macroscopic separation.

Before we proceed, however, there is another observation worth making. For bremsstrahlung in a sufficiently thin layer of substance, a fair approximation is the smallness of scattering angles (dipole limit), when  $(\mathbf{v}_1 - \mathbf{v}_2)^2 \ll 1 - v^2 = \gamma^{-2}$ . In that case, the structure of currents (4)–(5) appreciably simplifies. Linearizing  $\mathbf{J}_{21}$  in  $\mathbf{v}_{21} = \boldsymbol{\chi}_1$  and  $\mathbf{J}_{32}$  in  $\mathbf{v}_{32} = \boldsymbol{\chi}_2$ , integrating over radiation angles, and averaging (3b) over scattering angles

$\chi_1, \chi_2$  yields

$$\left\langle \frac{dI}{d\omega} \right\rangle = \left( \left\langle \frac{dI_1}{d\omega} \right\rangle + \left\langle \frac{dI_2}{d\omega} \right\rangle \right) \left( 1 + \frac{2\langle \chi_1 \cdot \chi_2 \rangle}{\langle \chi_1^2 \rangle + \langle \chi_2^2 \rangle} g_{\text{dd}}(\Omega) \right), \quad (9)$$

with

$$g_{\text{dd}}(\Omega) = \frac{3}{2} \int_0^\infty d\Theta^2 \frac{1 + \Theta^4}{(1 + \Theta^2)^4} \cos \Omega(1 + \Theta^2), \quad (10)$$

$\Omega = \frac{\omega t_{21}}{2\gamma^2}$ , and  $\Theta = \gamma\theta$ . Since in most cases, successive scatterings are not causally connected, the correlator in (9) reduces to a product of mean scattering angles:

$$\langle \chi_1 \cdot \chi_2 \rangle = \langle \chi_1 \rangle \cdot \langle \chi_2 \rangle.$$

For amorphous targets, mean deflection angles are obviously zero, wherefore the whole interference in the spectrum in this approximation vanishes. To preserve the interference effects between the targets, one thus needs either to render both scatterings asymmetric<sup>1</sup>, or to arrange *non-dipole* conditions for radiation in the amorphous target, which may be simpler to bring into practice, and will be the subject of our study in what follows.

### III. SPECTRUM OF NON-DIPOLE RADIATION FROM ONE PLATE

To make our presentation self-contained, before addressing interference effects in a composite target, let us recapitulate the properties of bremsstrahlung on a single amorphous foil. This section gives the account of relevant formulae, highlighting the differences between Gaussian and Molière averaging procedures, as well as between frameworks of different authors. We will also propose two our own recipes for incorporating Coulomb corrections, which give a reasonable balance between precision and simplicity for the addressed case.

Radiation spectrum at scattering to a definite angle of arbitrary size (which is small by absolute value, but may be sizable compared with the typical radiation angle  $\gamma^{-1}$ ) expresses by an integral (see, e.g., [23])

$$\frac{dI_1}{d\omega} = \left( \frac{e}{2\pi} \right)^2 \int d^2n (\mathbf{n} \times \mathbf{J}_{21})^2 = \frac{2e^2}{\pi} F(\gamma\chi/2), \quad (11)$$

where

$$F(\xi) = \frac{2\xi^2 + 1}{\xi\sqrt{\xi^2 + 1}} \ln \left( \xi + \sqrt{\xi^2 + 1} \right) - 1. \quad (12)$$

<sup>1</sup> Natural candidates for such deflectors could be magnets, but strong magnets with dimensions smaller than  $l_f$  are challenging to manufacture. More compact deflectors could be created with the aid of lasers, as proposed in [18], or bent crystals.

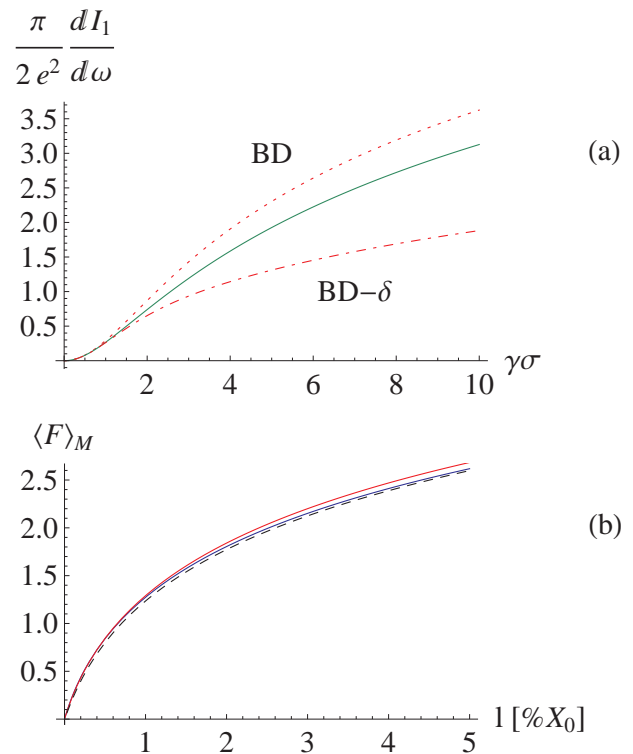


FIG. 1: (a) Green solid curve,  $\langle F \rangle_\sigma$  [Eq. (20) or (35)]; red dashed curve,  $F$  [Eq. (12) or Eq. (24)]; red dot-dashed curve, the corrected Blankenbecler-Drell approximation (27). (b) Red curve (upper); Molière averaging for gold, blue curve, Molière averaging for carbon; dashed curve, Gaussian averaging by Eq. (44).

Small-angle expansion of (12) can be obtained as

$$F(\xi) = - \sum_{n=1}^{\infty} \frac{(n-1)!(n+1)!}{(2n+1)!} (-4\xi^2)^n. \quad (13a)$$

$$= \frac{4}{3}\xi^2 - \frac{4}{5}\xi^4 + \dots = \frac{1}{3}(\gamma\chi)^2 - \frac{1}{20}(\gamma\chi)^4 + \dots \quad (13b)$$

Series (13a) has finite (actually, unit) convergence radius, which is natural in view of the presence in (12) of the structure  $\sqrt{\xi^2 + 1}$ .

The large-angle asymptotics of (12) is logarithmic:

$$F(\xi) \underset{\xi \rightarrow \infty}{\simeq} 2 \ln 2\xi - 1 = 2 \ln \gamma\chi - 1. \quad (14)$$

The logarithm here stems from the fact that although for a large-angle scattering, the radiation cones from the initial and final electron lines are well separated, the region between them is filled by an enhanced radiation, owing to the interference between the cones. It is integration over this inter-jet domain which gives rise to the large logarithm in (14).

### A. Gaussian averaging over scattering angles

Eqs. (11), (12) may be used to derive radiation spectrum in a thin layer of substance [under condition when a target thickness is much smaller than the photon formation length (1) in the considered range of  $\omega$ ]. To this end, (11) must be averaged with the appropriate distribution in scattering angles in the target [4, 9]. In the simplest approximation, this distribution can be taken to be Gaussian. Averaging over scattering angles with the Gaussian distribution with rms scattering angle  $\sigma$ ,

$$\frac{dw_\sigma}{d\chi^2} = \frac{1}{\sigma^2} e^{-\chi^2/\sigma^2}, \quad (15)$$

one gets

$$\left\langle \frac{dI_1}{d\omega} \right\rangle_\sigma = \frac{2e^2}{\pi} \langle F \rangle_\sigma, \quad (16)$$

where

$$\begin{aligned} \langle F \rangle_\sigma &= \int_0^\infty d\chi^2 \frac{1}{\sigma^2} e^{-\chi^2/\sigma^2} F(\gamma\chi/2) \\ &= \frac{8}{\gamma^2\sigma^2} \int_0^\infty d\xi \xi e^{-\frac{4\xi^2}{\gamma^2\sigma^2}} F(\xi). \end{aligned} \quad (17)$$

Inserting here (13a), and integrating termwise yields

$$\langle F \rangle_\sigma = - \sum_{n=1}^{\infty} \frac{(n-1)!n!(n+1)!}{(2n+1)!} (-\Sigma^2)^n, \quad (18)$$

with  $\Sigma = \gamma\sigma$ . Series (18) diverges for any finite  $\Sigma$  (not surprisingly since it was derived by integrating a series beyond its convergence domain); nonetheless, the sequence of its terms may be used as an asymptotic expansion.

The first two terms in Eq. (18) are

$$\langle F \rangle_\sigma \underset{\Sigma \ll 1}{\simeq} \frac{1}{3}\Sigma^2 - \frac{1}{10}\Sigma^4. \quad (19)$$

Note that the coefficient at the leading-order term is the same as in (13b), but the coefficient at the next-to-leading order term is twice greater.

To obtain large- $\Sigma$  asymptotics of  $\langle F \rangle_\sigma$ , it is advantageous to change in (17) the integration variable to  $\xi = \sinh \frac{w}{2}$ :

$$\begin{aligned} \langle F \rangle_\sigma &= \frac{2}{\Sigma^2} e^{\frac{2}{\Sigma^2}} \int_0^\infty dw e^{-\frac{2}{\Sigma^2} \cosh w} w \cosh w - 1 \\ &= e^{\frac{2}{\Sigma^2}} K_0 \left( \frac{2}{\Sigma^2} \right) - 1 \\ &\quad + \frac{2}{\Sigma^2} e^{\frac{2}{\Sigma^2}} \int_0^\infty dw w e^{-w - \frac{2}{\Sigma^2} \cosh w}. \end{aligned} \quad (20)$$

The remaining integral in (20) is a bounded function, ranging from 0 to 1. At large  $\Sigma$ , this term vanishes due to the pre-factor  $\Sigma^{-2}$ , so the corresponding asymptotics

of  $\langle F \rangle_\sigma$  is determined by that of Macdonald function at the origin:  $K_0(z) \underset{z \rightarrow 0}{\simeq} \ln \frac{2}{z} - \gamma_E$ . Employing this in (20), we get [9]

$$\langle F \rangle_\sigma \underset{\Sigma \gg 1}{\simeq} 2 \ln \Sigma - \gamma_E - 1. \quad (21)$$

### B. Blankenbecler's approximations

It is instructive to compare result (16)–(17) with representations derived within frameworks of Blankenbecler and Drell [14], and Baier and Katkov [16], under the same conditions of (geometrically) thin target and Gaussian scattering.

Blankenbecler's result [see [14], Eq. (30)] for the thin-target limit reads

$$F_B(T) = \int_0^1 dw \left( \frac{1+3T}{1+6Tw(1-w)} - 1 \right). \quad (22a)$$

Evaluation of this integral yields

$$F_B(T) = F \left( \sqrt{3T/2} \right), \quad (22b)$$

where  $F$  is given by Eq. (12). Hence, the correspondence between  $T$  and  $\Sigma$  is

$$T = \Sigma^2/6, \quad (23)$$

and the approximation of Blankenbecler consists in substituting the rms scattering angle to the non-averaged (fixed-scattering-angle) radiation spectrum:

$$F_B(T) = F(\Sigma/2). \quad (24)$$

This correspondence is what one could expect, given that Blankenbecler and Drell [6], similarly to Landau and Pomeranchuk [2], replaced an average of an oscillatory function in the integrand of a double time integral by the oscillatory function with average amplitude and phase. As is seen from comparison of asymptotics (21) and (14), however, such a simple-minded replacement deviates from the exact result only by  $\sim 15\%$ .

Yet another possible source of inaccuracy, though, may stem from the fact that for numerical calculations, Blankenbecler adopted relation

$$\langle Q_\perp^2 \rangle = \frac{2\pi m_e^2}{e^2} \frac{l}{X_0} \quad (25)$$

(with  $l$  the target thickness and  $X_0$  the radiation length). The coefficient in (25) differs by a constant factor 1/2 from that in the Rossi formula

$$\langle Q_\perp^2 \rangle = \frac{4\pi m_e^2}{e^2} \frac{l}{X_0}. \quad (26)$$

Accordingly, Blankenbecler defined the scaled target thickness [see [6], Eq. (10.1), [14], Eq. (16)]

$$T = \frac{\pi}{3\alpha} \frac{l}{X_0},$$

consistent with the correspondence rule (23). But physically, the coefficient in the relation between  $\langle Q_{\perp}^2 \rangle$  and  $l/X_0$  should vary logarithmically with  $l$ . More accurate description of multiple Coulomb scattering will be furnished in Sec. III D.

In [15], Blankenbecler derived a correction to Eq. (22a) [see [15], Eq. (109)]:

$$\tilde{F}_B(T) = \int_0^1 dw \left( \frac{1 + \frac{3}{2}T}{1 + 6Tw(1-w)} + \frac{\frac{3}{2}T}{[1 + 6Tw(1-w)]^2} - 1 \right). \quad (27)$$

At small  $T$ , i.e., small  $\Sigma$ , it rather neatly reproduces the next-to-leading order term in the exact small-angle expansion (19), provided one uses here the correspondence (23):

$$\tilde{F}_B(T) \underset{\Sigma \ll 1}{\simeq} 2T - \frac{33}{10}T^2 = \frac{1}{3}\Sigma^2 - \frac{11}{120}\Sigma^4. \quad (28)$$

However, at large  $\Sigma$  (or  $T$ ), approximation (27) fails by a factor of 2 [see Fig. 1(b), red dot-dashed curve], and can not be regarded as tenable there.

### C. Baier and Katkov's representation

Baier and Katkov's result for the case of one foil [16] reads<sup>2</sup>

$$F_{BK}(b) = \int_0^{\infty} \frac{dx}{x} e^{-x} \int_0^1 dw \left\{ 1 - \frac{1}{[1 + \frac{x}{b}w(1-w)]^2} \right\}. \quad (29)$$

Evaluation of this integral re-obtains expression (17), once one identifies

$$b = \Sigma^{-2}, \quad (30)$$

and

$$F_{BK}(\Sigma^{-2}) = \langle F \rangle_{\sigma}.$$

Baier and Katkov stated their own prescription for computation of  $b^{-1}$ , which will be compared with our prescription in the next subsection.

### D. Weighting with the Molière distribution. Impact parameter representation

For very thin targets, the distribution in scattering angles can significantly deviate from a Gaussian, while in

the extreme  $l \rightarrow 0$ , it must turn proportional to the differential cross-section of single scattering. To be more accurate, one may utilize the general (Molière) solution of the kinetic equation in terms of a Fourier-Bessel integral [24]:

$$\frac{dw_M}{d^2\chi} = \frac{1}{(2\pi)^2} \int d^2r e^{i\mathbf{r}\cdot\chi} e^{-nl \int d\sigma(\chi)[1-J_0(r\chi)]}, \quad (31)$$

where  $d\sigma(\chi)$  is the scattering differential cross-section. It may be noted that at substantial thicknesses, (31) is approximable by a Gaussian plus corrections [24], but we will not resort to such approximations here, dealing directly with the exact integral representation (31).

According to Eqs. (3b), (4),

$$\begin{aligned} \frac{dI}{d\omega} &= \left(\frac{e}{2\pi}\right)^2 \int d^2n \left( \frac{\mathbf{n} \times \mathbf{v}_1}{1 - \mathbf{n} \cdot \mathbf{v}_1} - \frac{\mathbf{n} \times \mathbf{v}_2}{1 - \mathbf{n} \cdot \mathbf{v}_2} \right)^2 \\ &= \left(\frac{e}{\pi}\right)^2 \int d^2n \left( \frac{\mathbf{n} - \mathbf{v}_1}{\gamma^{-2} + (\mathbf{n} - \mathbf{v}_1)^2} \right. \\ &\quad \left. - \frac{\mathbf{n} - \mathbf{v}_2}{\gamma^{-2} + (\mathbf{n} - \mathbf{v}_2)^2} \right)^2, \end{aligned} \quad (32)$$

where the last integral effectively extends over the transverse plane of small angle differences. Since the two terms in parentheses in (32) only differ by a shift in the  $\mathbf{n}_{\perp}$  plane, it may be expedient to expand them into Fourier integrals, so that the angular shift converts to a phase factor:

$$\frac{\mathbf{n} - \mathbf{v}}{\gamma^{-2} + (\mathbf{n} - \mathbf{v})^2} = \frac{i}{2\pi} \int d^2r e^{i(\mathbf{n}-\mathbf{v})\cdot\mathbf{r}} \frac{\partial}{\partial\mathbf{r}} K_0(r/\gamma). \quad (33)$$

Considering that  $\omega(\mathbf{n} - \mathbf{v})$  is the photon's transverse momentum,  $\mathbf{r}/\omega$  can be interpreted as the photon's impact parameter relative to the parent electron.

Inserting (33) to Eq. (32) obtains

$$\frac{dI}{d\omega} = \left(\frac{e}{\pi}\right)^2 \int d^2r \left[ \frac{\partial}{\partial\mathbf{r}} K_0(r/\gamma) \right]^2 \left| 1 - e^{i(\mathbf{v}_1 - \mathbf{v}_2)\cdot\mathbf{r}} \right|^2 \quad (34a)$$

$$= \frac{4e^2}{\pi\gamma^2} \int_0^{\infty} dr r K_1^2(r/\gamma) [1 - J_0(\chi r)]. \quad (34b)$$

It can be checked that evaluation of the integral in (34b) reproduces the explicit form (11), (12).

The reader familiar with the light-cone formalism [25] will recognize  $\frac{e}{\pi} \frac{\partial}{\partial\mathbf{r}} K_0(r/\gamma)$  as being (the low- $\omega$  approximation for) the electron-photon component of the electron wave function, with the vector index accounting for the photon polarization. In this spirit,  $\frac{e}{\pi} \frac{\partial}{\partial\mathbf{r}} K_0(r/\gamma) (1 - e^{i(\mathbf{v}_1 - \mathbf{v}_2)\cdot\mathbf{r}})$  amounts the complete wave function after electron scattering to a definite angle, and for  $\mathbf{v}_2 \neq \mathbf{v}_1$  this wave function differs from zero. Correspondingly, the integral of its modulus square gives the total probability of emission of a photon with energy  $\omega$ , i.e., the radiation spectrum. Interpretation of

<sup>2</sup> We restored factor  $x^{-1}$  missing in [16].

this kind may be noteworthy for intuitive understanding of the final results, albeit in this paper we will refrain from using it technically, and adhere to the standard formulation of classical electrodynamics.<sup>3</sup>

To proceed, when expression (34b) is averaged over scattering angles with a Gaussian distribution (15), it becomes

$$\begin{aligned} \left\langle \frac{dI}{d\omega} \right\rangle_{\sigma} &= \int d^2\chi \frac{dw_{\sigma}}{d^2\chi} \frac{dI}{d\omega} \\ &= \frac{4e^2}{\pi\gamma^2} \int_0^{\infty} dr r K_1^2(r/\gamma) \left(1 - e^{-\sigma^2 r^2/4}\right) \end{aligned} \quad (35)$$

On the other hand, averaging with Molière distribution (31) leads to the form

$$\left\langle \frac{dI}{d\omega} \right\rangle_{\text{M}} = \frac{4e^2}{\pi\gamma^2} \int_0^{\infty} dr r K_1^2(r/\gamma) \left\{ 1 - e^{-nl \int d\sigma(\chi)[1-J_0(r\chi)]} \right\}, \quad (36)$$

essentially coinciding with the result of Zakharov [7] (see also [8]). It is also in the spirit of Glauber form [31] for scattering of a high-energy composite quantum system. (It is not crucial that in our case the scattering is multiple, since it conserves the impact parameter, anyway.)

To use formula (36), we need further to specify the differential cross-section of scattering on one atom. The simplest model thereof is

$$nld\sigma(\chi) = 2\chi_c^2 \frac{\chi d\chi}{(\chi^2 + \chi_1^2)^2}, \quad (37)$$

where  $\chi_c^2 = \frac{4\pi n l Z^2 e^4}{p^2 v^2}$ , and  $\chi_1 = (pR)^{-1}$ , with  $R$  playing the role of the atomic screening radius. Inserting (37) to (36) gives

$$\left\langle \frac{dI}{d\omega} \right\rangle_{\text{M}} = \frac{4e^2}{\pi} \int_0^{\infty} d\rho \rho K_1^2(\rho) \left\{ 1 - e^{-\frac{\chi_c^2}{\chi_1^2} [1 - \rho\gamma\chi_1 K_1(\rho\gamma\chi_1)]} \right\}. \quad (38)$$

At practice, parameter  $\gamma\chi_1 = (m_e R)^{-1} \ll 1$ , so for any value of  $\frac{\chi_c^2}{\chi_1^2}$ , for description of radiation it is always legitimate to expand  $K_1(\rho\gamma\chi_1)$  in vicinity of the origin:  $1 - zK_1(z) \simeq \frac{z^2}{2} \left(\ln \frac{z}{2} + \frac{1}{2} - \gamma_E\right)$ .

To determine the precise value of  $\chi_1$ , one may note that in the limit of small  $l$ ,

$$\left\langle \frac{dI}{d\omega} \right\rangle_{\text{M}} \underset{l \rightarrow 0}{\simeq} \frac{2e^2\gamma^2\chi_c^2}{\pi} \int_0^{\infty} d\rho \rho^3 K_1^2(\rho) \times \left( \ln \frac{2}{\rho\gamma\chi_1} + \frac{1}{2} - \gamma_E \right) \quad (39a)$$

$$= \frac{4e^2\gamma^2\chi_c^2}{3\pi} \left( \ln \frac{1}{\gamma\chi_1} + \frac{7}{12} \right). \quad (39b)$$

On the other hand, by definition of the radiation length (in the approximation of complete screening), that must equal<sup>4</sup>

$$\left\langle \frac{dI}{d\omega} \right\rangle_{\text{M}} \underset{l \rightarrow 0}{\simeq} \frac{4l}{3X_0}. \quad (40)$$

Parameter  $\chi_1$  can thus be related to phenomenological parameters  $X_0$  and  $n$  via

$$\gamma\chi_1 = \exp\left(\frac{7}{12} - \frac{m_e^2}{4nZ^2e^6X_0}\right). \quad (41)$$

In this paper, our approach will be simply to employ relation (41) in Eq. (38). The factor  $\frac{\chi_c^2}{\chi_1^2}$  in the exponent can be expressed in terms of the ratio  $l/X_0$ :

$$\begin{aligned} \frac{\chi_c^2}{\chi_1^2} &= \frac{4\pi n l Z^2 e^4}{m_e^2 \gamma^2 \chi_1^2} = \frac{\pi l}{e^2 \gamma^2 \chi_1^2} \frac{4nZ^2 e^6}{m_e^2} \\ &= \frac{\pi}{e^2 \gamma^2 \chi_1^2} \frac{l}{\left(\ln \frac{1}{\gamma\chi_1} + \frac{7}{12}\right) X_0}. \end{aligned} \quad (42)$$

Therewith, we have only one adjustable parameter  $\gamma\chi_1$  (instead of two, for radiation with and without atom ionization or excitation). That parameter depends on the radiation length, which may include all the molecular binding and crystal structure effects. At practice, though,  $X_0$  itself is often inferred from calculations by formulas for bremsstrahlung on a free atom, neglecting the inter-atomic effects [11, 28, 29].

Utilizing the commonly used (calculated [29]) values for the radiation length, for gold we obtain  $\gamma\chi_1 = 0.048$ ,  $\frac{\chi_c^2}{\chi_1^2} = 5 \cdot 10^4 \frac{l}{X_0}$ , whereas for carbon,  $\gamma\chi_1 = 0.0064$ ,  $\frac{\chi_c^2}{\chi_1^2} = 1.9 \cdot 10^6 \frac{l}{X_0}$ . Note that if the screening radius is estimated from relation  $R = \frac{1}{m_e \gamma\chi_1}$ , for gold it amounts  $0.15a_B$ , while for carbon,  $1.14a_B$ . The presented estimates for  $R$  are generally greater than those following from the prescription used by Zakharov [7, 29]

$$\ln \frac{R}{a_B} = \ln \frac{a_{\text{el}}}{a_B} + \frac{1}{Z} \ln \frac{a_{\text{in}}}{a_B} = \ln(0.83Z^{-1/3}) + \frac{1}{Z} \ln(5.2Z^{-2/3}). \quad (43)$$

For gold, Eq. (43) gives  $R = 0.19a_B$ , while for carbon,  $R = 0.49a_B$ , the latter deviating distinctly from our above estimate. Fortunately, though, the sensitivity to this parameter is only logarithmic.

Fig. 1(b) overlays the predictions of Eq. (38) for carbon and for gold. Along with those, we plot formfactor (17) for Gaussian averaging with the rms scattering angle

<sup>3</sup> This attitude also saves us from encountering divergences, compared with [6, 7, 14, 16] where subtraction of divergent ‘vacuum’ terms from the final result was needed.

<sup>4</sup> Corrections to the complete screening approximation might be taken into account via a re-definition of  $X_0$  in Eq. (40).

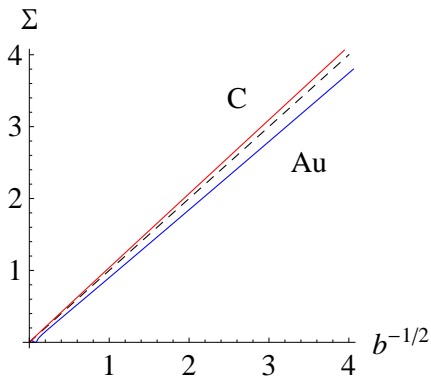


FIG. 2: Correspondence between values of rms scattering angle calculated by our Eq. (A2) and by Baier and Katkov's Eq. (45). Red curve – for carbon; blue curve – for gold. The auxiliary dashed line marks the diagonal  $\Sigma = b^{-1/2}$ .

evaluated by the widely used empirical formula<sup>5</sup> [26, 28]

$$\gamma\sigma = \frac{13.6 \text{ MeV}}{m_e} \sqrt{\frac{2l}{X_0}} \left( 1 + 0.038 \ln \frac{l}{X_0} \right). \quad (44)$$

Formula (44) is known to work with an accuracy better than 10% for  $l > 10^{-3}X_0$ . From Fig. 1(b) we conclude that for bremsstrahlung on one plate, the agreement is good in the whole range of  $l$ , including  $l < 10^{-3}X_0$ . That is natural since it can be shown that under some approximations, formula (44) can actually be derived from the rigorous representation (38) (see Appendix A).

Finally, our Eq. (A2) approximately accounting for Coulomb corrections in multiple scattering can also be compared with the recipe of Baier and Katkov [16]:

$$b^{-1} = \gamma^2 \chi_c^2 \left[ 2 \ln(183Z^{-1/3}) - 2(Z\alpha)^2 \sum_{k=1}^{\infty} \frac{1}{k(k^2 + (Z\alpha)^2)} + \ln b^{-1} \right]. \quad (45)$$

Predictions of Eq. (A2) and (45) are confronted in Fig. 2, and are reasonably close, although some differences are perceptible.

#### IV. TWO FOILS

We are now in a position to address the case of two plates. In Eq. (3b), the first two terms are individual

contributions from each plate, described by formulas of Sec. III, while the nontrivial third term of Eq. (3b) involves the product of currents induced by scattering in different plates. Hence, averaging of those currents over corresponding scattering angles proceeds independently:

$$\langle (\mathbf{n} \times \mathbf{J}_{21}) \cdot (\mathbf{n} \times \mathbf{J}_{32}) \rangle = (\mathbf{n} \times \langle \mathbf{J}_{21} \rangle) \cdot (\mathbf{n} \times \langle \mathbf{J}_{32} \rangle). \quad (46)$$

As was pointed out in the end of Sec. II, product (46) receives a suppression after integration over azimuthal directions of  $\mathbf{n}$ . Therefore, it is reasonable to carry out the averaging in two steps: First, to average over azimuths of  $\mathbf{n}$ , which does not need a reference to a specific form of the (axially-symmetric) scattering angle distribution function. At the second step, one implements convolutions with specific angular distribution functions.

##### A. Azimuthal averaging for the interference term

Granted that the currents entering Eq. (3) have similar structure, it suffices to consider a generic form

$$\mathbf{J} = \frac{\mathbf{v}_2}{1 - \mathbf{n} \cdot \mathbf{v}_2} - \frac{\mathbf{v}}{1 - \mathbf{n} \cdot \mathbf{v}}, \quad (47)$$

where  $\mathbf{v}$  may equal  $\mathbf{v}_1$  or  $\mathbf{v}_3$ . Averaging of expression (47) over azimuths of the scattering angle, say, wrt direction  $\mathbf{v}_2$  (it makes no difference since ultimately all directions are to be integrated over) proceeds as follows. Decomposing  $\mathbf{v}$  into components parallel and orthogonal to  $\mathbf{v}_2$ ,

$$\mathbf{v} = \mathbf{v}_{\parallel} + \mathbf{v}_{\perp}, \quad (48)$$

with  $\mathbf{v}_{\perp} \perp \mathbf{v}_2 \parallel \mathbf{v}_{\parallel}$ , we compute the azimuthal average:

$$\begin{aligned} & \left\langle \frac{\mathbf{v}_{\parallel} + \mathbf{v}_{\perp}}{1 - \mathbf{n}_{\parallel} v_{\parallel} - \mathbf{n}_{\perp} \cdot \mathbf{v}_{\perp}} \right\rangle_{\text{azim } \mathbf{v}_{\perp}} \\ &= \frac{1}{2\pi} \int_{-\pi}^{\pi} d\phi \frac{\mathbf{v}_{\parallel} + \frac{\mathbf{n}_{\perp}}{n_{\perp}} v_{\perp} \cos \phi}{1 - n_{\parallel} v_{\parallel} - n_{\perp} v_{\perp} \cos \phi} \\ &= \frac{\mathbf{v}_{\parallel} + \frac{\mathbf{n}_{\perp}}{n_{\perp}} (1 - n_{\parallel} v_{\parallel})}{\sqrt{(1 - n_{\parallel} v_{\parallel})^2 - n_{\perp}^2 v_{\perp}^2}} - \frac{\mathbf{n}_{\perp}}{n_{\perp}^2}. \end{aligned} \quad (49)$$

Now we can insert  $\mathbf{n}_{\perp} = \mathbf{n} - \mathbf{n}_{\parallel} = \mathbf{n} - \mathbf{v}_2 \frac{n_{\parallel}}{v_2}$ , and omit the component parallel to  $\mathbf{n}$ , which does not contribute to the vector product with  $\mathbf{n}$  appearing in Eq. (46). As a result, the azimuthally averaged radiation amplitude assumes the form

$$\mathbf{n} \times \langle \mathbf{J} \rangle_{\text{azim } \mathbf{v}_{\perp}} = \frac{\mathbf{n} \times \mathbf{v}_2}{v_2} 4\gamma^2 G(\Sigma, X), \quad (50)$$

with

$$4\gamma^2 G = \frac{1}{1 - n_{\parallel} v_2} - \frac{1}{n_{\perp}^2} \left( n_{\parallel} - \frac{n_{\parallel} - v_{\parallel}}{\sqrt{(1 - n_{\parallel} v_{\parallel})^2 - n_{\perp}^2 v_{\perp}^2}} \right).$$

<sup>5</sup> More elaborate empirical formulas taking into account  $Z$ -dependence of the coefficient were obtained [27], but to keep the treatment simple, and expose numerical differences between the approaches, we will confine ourselves here to parameterization (44).



In the small-angle approximation,  $n_{\perp} = \theta \ll 1$ ,  $v_{\perp} = \chi \ll 1$ ,  $n_{\parallel} = 1 - \theta^2/2$ ,  $v_{\parallel} = 1 - (\gamma^{-2} + \chi^2)/2$ , we obtain

$$G \approx \frac{1}{2(1+\gamma^2\theta^2)} - \frac{1}{4\gamma^2\theta^2} \left( 1 + \frac{\theta^2 - \chi^2 - \gamma^{-2}}{\sqrt{[\gamma^{-2} + (\theta - \chi)^2][\gamma^{-2} + (\theta + \chi)^2]}} \right) \equiv \frac{1}{2(1+\Theta^2)} - \frac{1}{4\Theta^2} \left( 1 + \frac{\Theta^2 - X - 1}{\sqrt{(X+1-\Theta^2)^2 + 4\Theta^2}} \right) \quad (51)$$

$X = \gamma^2\chi^2$ . Function (51) is everywhere positive. At small  $\Theta$ , it expands as

$$G = \frac{1}{2} \sum_{n=0}^{\infty} \Theta^{2n} \left\{ (-1)^n + \frac{1}{2(X+1)^{n+1}} \left[ P_{n+1} \left( \frac{X-1}{X+1} \right) - P_n \left( \frac{X-1}{X+1} \right) \right] \right\} \underset{\Theta \ll 1}{\approx} \frac{1}{2} - \frac{1}{2(1+X)^2} + \mathcal{O}(\Theta^2), \quad (52)$$

where  $P_n$  are Legendre polynomials [30] arising as coefficients in the expansion  $(1 - 2\zeta h + h^2)^{-1/2} = \sum_{n=0}^{\infty} P_n(\zeta) h^n$ .

Before proceeding to averaging over moduli of scattering angles, i.e.,  $X$ , it is also instructive to examine the asymptotics of  $G$  as a function of  $X$ . At small  $X$ ,

$$G = \frac{1}{4\Theta^2} \sum_{n=0}^{\infty} \frac{X^{n+1}}{(\Theta^2+1)^{n+1}} \left[ P_n \left( \frac{\Theta^2-1}{\Theta^2+1} \right) - \frac{\Theta^2-1}{\Theta^2+1} P_{n+1} \left( \frac{\Theta^2-1}{\Theta^2+1} \right) \right] \quad (53a)$$

$$\underset{X \ll 1}{\approx} \frac{1}{(1+\Theta^2)^3} X + \mathcal{O}(X^2). \quad (53b)$$

Here the leading term is proportional to  $X \propto \chi^2$ , whereas in the dipole approximation the current is  $\propto \chi$ , but the latter contribution vanishes after azimuthal averaging [see Eq. (9)]. Thus, the leading term (53b) corresponds to a ‘‘quadrupole’’ approximation.

On the other hand, at large  $\chi$  and fixed  $\theta$ ,

$$G \underset{X \gg 1}{\approx} \begin{cases} \frac{1}{2(1+\Theta^2)} & (\theta < \chi) \\ 0 & (\theta > \chi) \end{cases}. \quad (54)$$

Factor  $\frac{1}{2(1+\Theta^2)}$  here describes the radiation from the  $\mathbf{v}_2$  half-line alone. As for the radiation from the  $\mathbf{v}$  half-line, it is smeared by the azimuthal averaging, but in any case, the inter-jet region extends only out to polar angle  $\theta \approx \chi$ . It is noteworthy that function  $G$  features no enhancement around  $\theta = \chi$ , which could be expected due to the presence of the  $\mathbf{v}$ -jet. So, after the azimuthal averaging, the latter jet does not manifest itself as a peak. For  $\theta > \chi$ , the radiation is suppressed because radiation amplitudes from  $\mathbf{v}_2$  and  $\mathbf{v}$  lines strongly cancel.

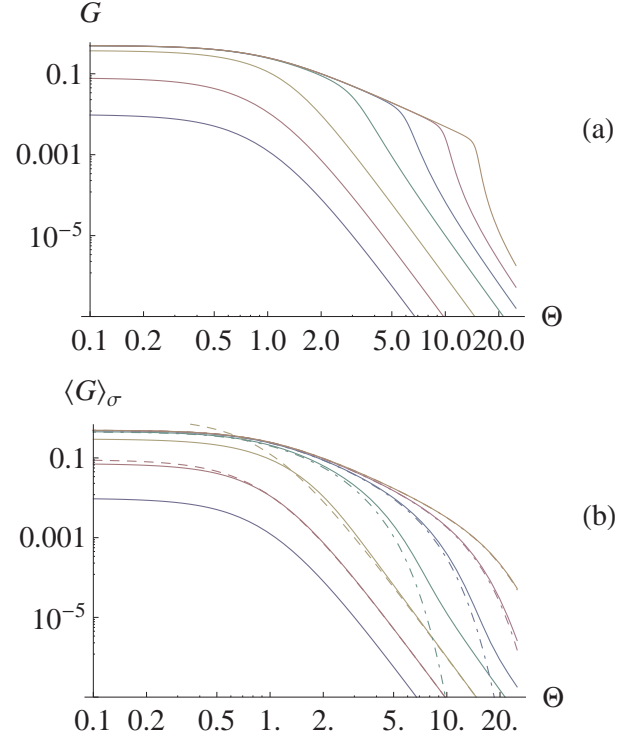


FIG. 3: (a) LogLog plot of the azimuthally averaged electromagnetic current at one scattering, Eq. (51), for scattering angles  $\gamma\chi = 0.1, 0.3, 1, 3, 6, 10, 15$  (solid curves, bottom to top). Dashed curves, approximation (53b); (b) Same for the Gaussian-weighted azimuthally averaged electromagnetic current at one scattering, Eq. (62b). Dashed curves, approximation (63b). Dot-dashed curves, approximation (64).

## B. The aggregate spectrum

Employing representation Eq. (50) in Eq. (46), we have

$$(\mathbf{n} \times \langle \mathbf{J}_{21} \rangle) \cdot (\mathbf{n} \times \langle \mathbf{J}_{32} \rangle) = -16\gamma^4\theta^2 \langle G \rangle_1 \langle G \rangle_2, \quad (55)$$

where

$$\langle G \rangle_i = \int_0^{\infty} d\chi^2 \frac{dw_i}{d\chi^2} G(\chi, \theta), \quad (56)$$

and we invoked the identity  $(\mathbf{n} \times \mathbf{v}_2)^2 = \theta^2$ . The minus sign in Eq. (56), i.e., the negativity of interference between the currents, retraces to the general property of saturation of radiation. In Eq. (3b), though, factor (55) is multiplied by an  $\omega$ -dependent factor  $\cos \Phi$ , and the corresponding product is yet to be integrated over polar radiation angles. Given that  $\cos \Phi$  is sign-alternating, the spectrum may then actually oscillate with the increase of  $\Omega$ , not only experience a suppression. Combining with the previously computed bremsstrahlung contributions

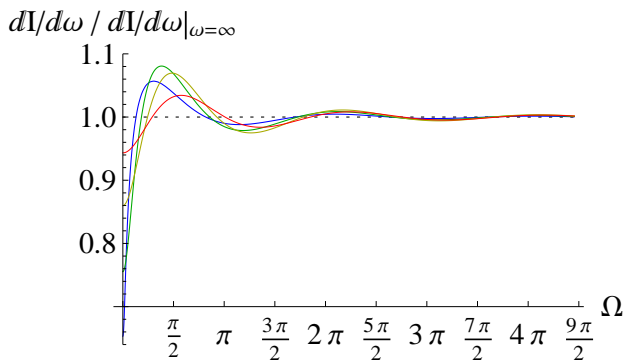


FIG. 4: Oscillations of spectrum of the bremsstrahlung on two foils, computed for Gaussian scattering-angle distribution functions with rms  $\Sigma_1 = \Sigma_2 = 0.5$  (thin red curve), 1 (yellow), 2 (green), 5 (blue). At  $\Omega \gtrsim \frac{t_{21}}{\max\{l_1, l_2\}}$ , the spectrum must rise again, and reach the Bethe-Heitler constant value (see Sec. VI).

from individual plates, which are  $\omega$ -independent, we get

$$\left\langle \frac{dI}{d\omega} \right\rangle = \frac{2e^2}{\pi} \left[ \langle F \rangle_1 + \langle F \rangle_2 - 4 \int_0^\infty d\Theta^2 \Theta^2 \langle G \rangle_1 \langle G \rangle_2 \cos \Omega(1 + \Theta^2) \right]. \quad (57)$$

The dependence of function (57) on  $\Omega$  is shown in Fig. 4. As anticipated, it exhibits an oscillatory behavior.

To determine the magnitude and the phase of the oscillations, note that at  $\Omega \gg 1$ , the integral in the last term of (57) is dominated by the vicinity of the lower endpoint, and its evaluation with  $\langle G \rangle_{1,2}(\Theta) = \langle G \rangle_{1,2}(0) + \mathcal{O}(\Theta^2)$  yields the asymptotics

$$\left\langle \frac{dI}{d\omega} \right\rangle \underset{\Omega \rightarrow \infty}{\simeq} \frac{2e^2}{\pi} \left[ \langle F \rangle_1 + \langle F \rangle_2 + \frac{4 \cos \Omega}{\Omega^2} \langle G \rangle_1(0) \langle G \rangle_2(0) + \mathcal{O}(\Omega^{-3}) \right]. \quad (58)$$

According to this result, maxima of  $dI/d\omega$  should appear at

$$\Omega \approx 2\pi n, \quad (59)$$

with  $n$  integer, independently of shapes of distribution functions  $\langle G \rangle$ . That simple prediction is confirmed by Fig. 4. A suggestive geometrical interpretation for the rule (59), in the spirit of wave optics, is that the maxima correspond to situations when the distance between the plates equals an integer number of full coherence lengths  $2\pi l_f$ .

Concerning the main maximum (which accounts for the bulk of the anti-LPM enhancement), however, there is no possibility to associate it with the case of unit wavelength shift as proposed in [14]. For  $\Omega \lesssim 1$ , of course,

formula (58) does not apply, but from the point of exact formula (57), the main maximum of  $dI/d\omega$  emerges when in the integrand of the last term, the maximum of<sup>6</sup>  $\Theta^2 \langle G \rangle_1(\Theta) \langle G \rangle_2(\Theta)$ , achieved at some  $\Theta = \Theta_*(\Sigma)$ , coincides with the extremum of  $\cos \Omega(1 + \Theta^2)$ :

$$\Omega_* = \frac{\pi}{1 + \Theta_*^2}, \quad (60)$$

whereat  $\cos \Theta_* < 0$ . This situation has to be discriminated from the case  $\Omega = \pi$  in Eq. (58), where the existence of a maximum for  $\Theta^2 \langle G \rangle_1 \langle G \rangle_2$  is irrelevant because there are several oscillations within its width, and the region of dominant contribution shifts to the endpoint. In the latter case, the half-wavelength shift corresponds to a spectral *minimum* next to the main maximum. As opposed to that, case (60) with the account of the denominator  $1 + \Theta_*^2$  can be called the inclined half-length, which is numerically close to quarter-wavelength.

It is worth stressing in this regard that although there is a denominator in relation (60) depending on  $\Sigma$ , but it obeys a relation  $\Theta_*(\Sigma) \lesssim 1$ . Clearly, even at large  $\Sigma$ , the contributing  $\Theta$  in Eq. (57) are  $\Theta \lesssim 1$ , i.e.,  $\theta \lesssim \gamma^{-1}$  with respect to the direction  $\mathbf{v}_2$ . Therefore, the use of the in-medium coherence length [32]

$$l_c(\omega, \Sigma) = \frac{l_f(\omega)}{1 + \Sigma^2} \quad (61)$$

in the resonance condition  $t_{21} \propto l_c(\omega, \Sigma)$  is *unjustified*. In fact, employment of (61) in application to the present problem led in [16] to a large underestimate of the location of the first spectral maximum.

Finally, one must pay attention to the pronounced spectral minimum at  $\omega = 0$ , which must be associated with zero wavelength shift. This limit is known to correspond to a situation when the radiation amplitude completely factorizes from the scattering one, and so radiation on two plates becomes the same as on one plate with the aggregate thickness. Such a relation may be not immediately transparent from Eq. (57), although proves by straightforward integration; we will also supply a simpler derivation thereof in Sec. V A.

### C. Weighting with Gaussian distribution

To deduce all the consequences from the averaging, let us now assume  $\frac{d\omega}{d^2x}$  in (56) to be a Gaussian weighting distribution (15). The averaging of  $G$  with such a distri-

<sup>6</sup> The existence of a maximum for this expression at non-zero  $\Theta$  owes in particular to the factor  $\Theta^2$ , which is due to the cancellation of interference effects at small  $\Theta$  – see the end of Sec. II.

bution simplifies after an integration by parts:

$$\begin{aligned}\langle G \rangle_\sigma(\Theta) &= \int_0^\infty d\chi^2 \frac{1}{\sigma^2} e^{-\chi^2/\sigma^2} G \\ &\equiv \int_0^\infty d\chi^2 e^{-\chi^2/\sigma^2} \frac{\partial}{\partial \chi^2} G\end{aligned}\quad (62a)$$

$$= \int_0^\infty dX \frac{e^{-X/\Sigma^2}}{[(X+1-\Theta^2)^2 + 4\Theta^2]^{3/2}}. \quad (62b)$$

The behavior of function (62b) is illustrated in Fig. 3(b) for several values of  $\Sigma$ . It is largely similar to that of  $G$  shown in Fig. 3(a), but is smoother at  $\Theta \sim \Sigma \gg 1$ , the latter property being natural inasmuch as the unit step function in (54) is smoothed out by the averaging over  $\chi$ .

Numerically, Eq. (57) with entries (20), (62b) proves to be equivalent to Eqs. (2.34), (2.36) of [16] under the correspondence rule (30), although analytically, the equivalence of both approaches is challenging to verify. Our representation seems to be better suited for the analytic study of  $\Sigma$ - and  $\Omega$ -dependences. With its aid, we will now derive small- and large- $\Sigma$  asymptotics of function  $\langle G \rangle_\sigma$ , which will be useful in what follows.

At small  $\Sigma$ , plugging expansion (53a) to Eq. (62a), and integrating termwise, we obtain

$$\begin{aligned}\langle G \rangle_\sigma(\Theta) &= \frac{1}{4\Theta^2} \sum_{n=0}^{\infty} \frac{(n+1)! \Sigma^{2(n+1)}}{(\Theta^2+1)^{n+1}} \left[ P_n \left( \frac{\Theta^2-1}{\Theta^2+1} \right) \right. \\ &\quad \left. - \frac{\Theta^2-1}{\Theta^2+1} P_{n+1} \left( \frac{\Theta^2-1}{\Theta^2+1} \right) \right]\end{aligned}\quad (63a)$$

$$\underset{\Sigma \ll 1}{\approx} \Sigma^2 (1 + \Theta^2)^{-3} + \mathcal{O}(\Sigma^4). \quad (63b)$$

Similarly to Eq. (18), expansion (63a) diverges, but again, it remains sensible as an asymptotic series. Its leading term (63b) coincides with the asymptotics of non-averaged expression (53b), granted that there the  $\chi$ -dependence factorizes. The behavior of approximation (63b) is shown in Fig. 3(b) by dashed curves.

On the other hand, at significant  $\Sigma$ , it is legitimate to expand  $e^{-X/\Sigma^2}$  to Taylor series in vicinity of point  $X = \Theta^2 - 1$  and integrate termwise:

$$\begin{aligned}\langle G \rangle_\sigma(\Theta) &\underset{\Sigma \gg 1}{\approx} e^{-\frac{\Theta^2-1}{\Sigma^2}} \int_0^\infty dX \frac{1}{[(X+1-\Theta^2)^2 + 4\Theta^2]^{3/2}} \\ &\quad \times \left( 1 + \frac{\Theta^2-1-X}{\Sigma^2} \right) \\ &= \frac{1}{1+\Theta^2} e^{-\frac{\Theta^2-1}{\Sigma^2}} \left( \frac{1}{2} - \frac{1}{\Sigma^2} \right) \\ &\approx \frac{1}{2(1+\Theta^2)} e^{-\frac{1+\Theta^2}{\Sigma^2}}.\end{aligned}\quad (64)$$

According to Fig. 3(b) (dot-dashed curves), approximation (64) works well for  $\Sigma > 3$ . At large  $\Sigma$  and fixed  $\Theta$ , the exponential here tends to unity, and form (54) is retrieved.

#### D. Averaging with Molière distribution. Impact parameter representation

If instead of a Gaussian we prefer to use Molière weighting distribution (31), it may be more convenient to return to Eq. (3b) for the radiation spectrum. In the last line of Eq. (3b), the product of currents consists of 4 terms, which have similar structure. It suffices to calculate only one of those,

$$\begin{aligned}O_{13} &= \int d^2 n \frac{\mathbf{n} - \mathbf{v}_1}{\gamma^{-2} + (\mathbf{n} - \mathbf{v}_1)^2} \cdot \frac{\mathbf{n} - \mathbf{v}_3}{\gamma^{-2} + (\mathbf{n} - \mathbf{v}_3)^2} \\ &\quad \times \cos \frac{\omega t_{21}}{2} [\gamma^{-2} + (\mathbf{n} - \mathbf{v}_2)^2],\end{aligned}\quad (65)$$

while the other terms can be reconstructed by replacements  $\mathbf{v}_3 \rightarrow \mathbf{v}_2$  or/and  $\mathbf{v}_1 \rightarrow \mathbf{v}_2$ .

Changing the integration variable to  $\mathbf{n}'_\perp = \mathbf{n} - \mathbf{v}_2$ , inserting representations (33) for the first factor in the first line of (81), and a complex conjugate representation for the second factor, one brings it to the form of an integral over impact parameters:

$$\begin{aligned}O_{13} &= \int d^2 r_1 e^{i(\mathbf{v}_2 - \mathbf{v}_1) \cdot \mathbf{r}_1} \frac{\partial}{\partial \mathbf{r}_1} K_0(r_1/\gamma) \\ &\quad \cdot \int d^2 r_3 e^{i(\mathbf{v}_3 - \mathbf{v}_2) \cdot \mathbf{r}_3} \frac{\partial}{\partial \mathbf{r}_3} K_0(r_3/\gamma) \\ &\quad \times \Re \mathfrak{K} S_\omega(\mathbf{r}_1 - \mathbf{r}_3, t_{21}).\end{aligned}\quad (66)$$

Here

$$S_\omega(\mathbf{r}_1 - \mathbf{r}_3, t_{21}) = \frac{1}{(2\pi)^2} \int d^2 n'_\perp e^{i\mathbf{n}'_\perp \cdot (\mathbf{r}_1 - \mathbf{r}_3) - i\frac{\omega t_{21}}{2}(\gamma^{-2} + \mathbf{n}'_\perp{}^2)} \quad (67)$$

may be regarded as Green's function for a two-dimensional free Schrödinger equation on the light front:

$$\begin{aligned}\left[ \frac{\omega}{2} \left( \gamma^{-2} - \frac{\partial^2}{\partial (\mathbf{r}_1 - \mathbf{r}_3)^2} \right) - i \frac{\partial}{\partial t_{21}} \right] S_\omega(\mathbf{r}_1 - \mathbf{r}_3, t_{21}) \Theta(t_{21}) \\ = -i \delta(\mathbf{r}_1 - \mathbf{r}_3) \delta(t_{21}),\end{aligned}\quad (68)$$

and it evaluates in closed form:

$$\Re \mathfrak{K} S_\omega(\mathbf{r}_1 - \mathbf{r}_3, t_{21}) = \frac{1}{2\pi\omega t_{21}} \sin \left[ \frac{(\mathbf{r}_1 - \mathbf{r}_3)^2}{2\omega t_{21}} - \frac{\omega t_{21}}{2\gamma^2} \right]. \quad (69)$$

Note that this function depends only on the difference between  $\mathbf{r}_1$  and  $\mathbf{r}_3$ , just as in (57) the cosine depends, besides  $\omega t_{21}$ , only on the angle between  $\mathbf{v}_2$  and  $\mathbf{n}$ .

Restoring the rest of the interference terms by substitutions  $\mathbf{v}_1 \rightarrow \mathbf{v}_2$  or  $\mathbf{v}_3 \rightarrow \mathbf{v}_2$ , and combining them, we get

$$\begin{aligned}\frac{dI}{d\omega} &= \frac{dI_1}{d\omega} + \frac{dI_2}{d\omega} \\ &+ \frac{2e^2}{\pi^2} \int d^2 r_1 d^2 r_3 \left( 1 - e^{i(\mathbf{v}_1 - \mathbf{v}_2) \cdot \mathbf{r}_1} \right) \left( 1 - e^{i(\mathbf{v}_2 - \mathbf{v}_3) \cdot \mathbf{r}_3} \right) \\ &\quad \times \frac{\partial}{\partial \mathbf{r}_1} K_0(r_1/\gamma) \cdot \frac{\partial}{\partial \mathbf{r}_3} K_0(r_3/\gamma) \Re \mathfrak{K} S_\omega(\mathbf{r}_1 - \mathbf{r}_3, t_{21})\end{aligned}\quad (70)$$

Convolving this with the Molière distribution function, and integrating over azimuths of  $\mathbf{r}_1$  and  $\mathbf{r}_3$ , leads to the result

$$\begin{aligned} \left\langle \frac{dI}{d\omega} \right\rangle_M &= \left\langle \frac{dI_1}{d\omega} \right\rangle_M + \left\langle \frac{dI_2}{d\omega} \right\rangle_M \\ &+ \frac{2e^2}{\pi\Omega} \int_0^\infty d\rho_1 \rho_1 K_1(\rho_1) \left\{ 1 - e^{-n_1 l_1 \int d\sigma(\chi)[1-J_0(\rho_1 \gamma \chi)]} \right\} \\ &\times \int_0^\infty d\rho_3 \rho_3 K_1(\rho_3) \left\{ 1 - e^{-n_2 l_2 \int d\sigma(\chi)[1-J_0(\rho_3 \gamma \chi)]} \right\} \\ &\times \cos \left( \frac{\rho_1^2 + \rho_3^2}{4\Omega} - \Omega \right) J_1 \left( \frac{\rho_1 \rho_3}{2\Omega} \right), \quad (71) \end{aligned}$$

where for convenience we rescaled the impact parameter variable to  $\rho_{1,3} = r_{1,3}/\gamma$ . Note that after integration over the azimuth, the dependence only on the impact parameter difference is somewhat disguised.

At large  $\Omega$ , upon approximations  $\cos \left( \frac{\rho_1^2 + \rho_3^2}{4\Omega} - \Omega \right) \rightarrow \cos \Omega$ ,  $J_1 \left( \frac{\rho_1 \rho_3}{2\Omega} \right) \rightarrow \frac{\rho_1 \rho_3}{4\Omega}$ , (71) factorizes:

$$\begin{aligned} \left\langle \frac{dI}{d\omega} \right\rangle_M &\xrightarrow{\Omega \rightarrow \infty} \left\langle \frac{dI_1}{d\omega} \right\rangle_M + \left\langle \frac{dI_2}{d\omega} \right\rangle_M \\ &+ \frac{e^2 \cos \Omega}{2\pi\Omega^2} \int_0^\infty d\rho_1 \rho_1^2 K_1(\rho_1) \left\{ 1 - e^{-n_1 l_1 \int d\sigma(\chi)[1-J_0(\rho_1 \gamma \chi)]} \right\} \\ &\times \int_0^\infty d\rho_3 \rho_3^2 K_1(\rho_3) \left\{ 1 - e^{-n_2 l_2 \int d\sigma(\chi)[1-J_0(\rho_3 \gamma \chi)]} \right\} \quad (72) \end{aligned}$$

This form proves to be equivalent to Eq. (58), by virtue of the identity

$$\frac{1}{4} \int_0^\infty d\rho \rho^2 K_1(\rho) \left\{ 1 - e^{-n l \int d\sigma(\chi)[1-J_0(\rho \gamma \chi)]} \right\} \quad (73a)$$

$$\begin{aligned} &= \frac{1}{4} \int d^2 \chi \frac{dw_M}{d^2 \chi} \int_0^\infty d\rho \rho^2 K_1(\rho) [1 - J_0(\rho \gamma \chi)] \\ &= \int d^2 \chi \frac{dw_M}{d^2 \chi} \left[ \frac{1}{2} - \frac{1}{2(1+X)^2} \right] \equiv \langle G \rangle_M(0) \quad (73b) \end{aligned}$$

[cf. Eq. (52)].

## V. ANALYSIS OF THE INTERFERENCE PATTERN

The spectrum of radiation on two plates that we have evaluated, even under the simplification of a negligible plate thicknesses, is a function of 3 variables:  $\Sigma_1$ ,  $\Sigma_2$ , and  $\Omega$ . In limiting cases, though, it reduces to simpler functions, which will be scrutinized below.

### A. Visibility of the low- $\omega$ dip

For experimental tests, it is imperative to estimate visibilities of gross features of the spectrum, and find their optimum by choosing appropriate foil materials and their

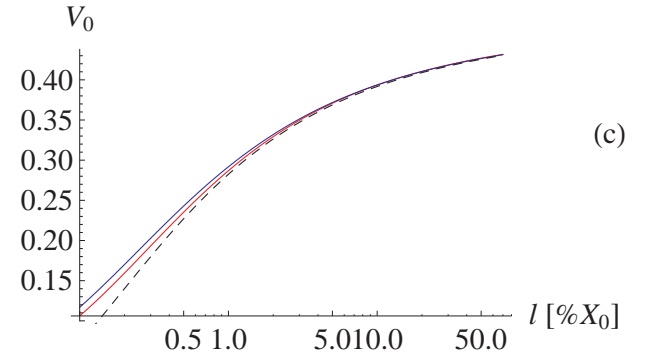
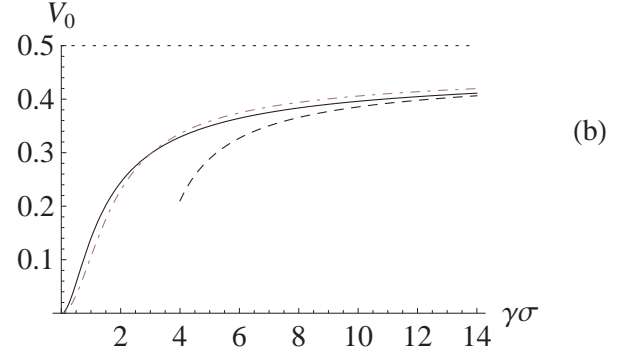
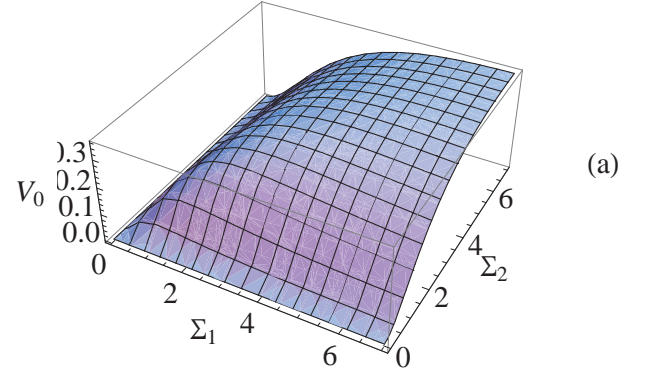


FIG. 5: The visibility of the low- $\omega$  dip, Eq. (75b). (a) For Gaussian averaging and arbitrary  $\Sigma_1$ ,  $\Sigma_2$ . (b) For Gaussian averaging and  $\Sigma_1 = \Sigma_2 = \Sigma$ . Solid black curve, exact expression (75). Dashed black curve, its asymptotics (77). Purple dot-dashed curve, the visibility in the Blankenbecler-Drell approximation. (c) For Molière averaging. Blue curve, carbon; red curve, gold; black dashed curve, Gaussian averaging with rms scattering angle computed by formula (44).

thicknesses. The interference term reaches its largest absolute value at  $\omega = 0$ . Therefore, it is natural to consider the characteristic quantity

$$V_0(\Sigma_1, \Sigma_2) = 1 - \left\langle \frac{dI}{d\omega} \right\rangle \Big|_{\omega=0} / \left\langle \frac{dI}{d\omega} \right\rangle \Big|_{\omega=\infty}. \quad (74)$$

Adopting the terminology from optics, this may be called the visibility of the low- $\omega$  dip. With the aid of Eq. (57), it can be explicitly written as

$$V_0 = \frac{4 \int_0^\infty d\Theta^2 \Theta^2 \langle G \rangle_1(\Theta) \langle G \rangle_2(\Theta)}{\langle F \rangle_1 + \langle F \rangle_2}. \quad (75a)$$

As we already mentioned at the end of Sec. IV B, here the spectrum must reduce to that from a single plate of aggregate thickness. This can now be proven rather easily, based on the impact parameter representation (71). There,  $S_\omega \xrightarrow{\Omega \rightarrow 0} \delta(\mathbf{r}_1 - \mathbf{r}_3)$ , and terms  $\frac{dI_1}{d\omega}$ ,  $\frac{dI_2}{d\omega}$  cancel with some of the interference terms, leaving  $\frac{dI}{d\omega} \xrightarrow{\Omega \rightarrow 0} \frac{dI_{l_1+l_2}}{d\omega}$ . Thereby,  $V_0$  indeed reduces to the form

$$V_0 = 1 - \frac{\langle F \rangle_{l_1+l_2}}{\langle F \rangle_1 + \langle F \rangle_2}. \quad (75b)$$

At small  $\Sigma$ ,

$$V_0 \underset{\Sigma_{1,2} \ll 1}{\simeq} \frac{3}{5} \frac{1}{\Sigma_1^{-2} + \Sigma_2^{-2}}, \quad (76)$$

i.e., essentially it is proportional to the minimal among  $\Sigma_1^2$ ,  $\Sigma_2^2$ .

At large  $\Sigma_1$ ,  $\Sigma_2$ ,

$$V_0 \underset{\Sigma_{1,2} \gg 1}{\simeq} \frac{1}{2} - \frac{\ln(\Sigma_1/\Sigma_2 + \Sigma_2/\Sigma_1)}{2(\ln \Sigma_1 \Sigma_2 - \gamma_E - 1)}. \quad (77)$$

Thus, in principle, asymptotically  $V_0$  tends to  $\frac{1}{2}$ . That is natural, inasmuch as radiation at one plate saturates as a function of its thickness, and hence the radiation at any two strongly scattering foils must be about twice stronger than on one of them. But practically, such a saturation is achieved only logarithmically, and is too remote, so the second term in Eq. (77) is usually significant.

The behavior of (75) and asymptotic approximation (77) is illustrated in Fig. 5(b) by black solid and dashed curves. For comparison, the purple dot-dashed curve also shows the corresponding result for Blankenbecler's theory, when in Eq. (75b)  $\langle F \rangle_\sigma$  is replaced by  $F(\Sigma/2)$ . Notably, that curve intersects with the exact result at  $\Sigma \approx 3$ , and keeps close to it at greater  $\Sigma$ . But at  $\Sigma \sim 1$  the difference is relatively large. It is also interesting to note that the Blankenbecler-Drell prediction for  $V_0$  is lower than the exact one, i.e., the neglect of fluctuations leads to an underestimation of the interference effect in radiation. That means that under the conditions of cancellation of dipole contributions in the interference, fluctuations help creating uncompensated contributions.

Likewise, it is useful to compare in this limit the predictions of Gaussian and Molière averaging [see Fig. 5(c)]. It appears that the Gaussian averaging prediction becomes inaccurate at  $l \lesssim 10^{-3} X_0$ , just where the accuracy of approximation (44) itself becomes worse than 10%.

## B. Visibility of secondary minima and maxima

In the opposite limit of large  $\omega$ , according to Eq. (58), the visibility may be characterized by the ratio

$$V_\infty(\Sigma_1, \Sigma_2) = \frac{4 \langle G \rangle_1(0) \langle G \rangle_2(0)}{\langle F \rangle_1 + \langle F \rangle_2}. \quad (78)$$

At small  $\Sigma$ , this quantity behaves as

$$V_\infty \simeq \frac{12}{\Sigma_1^{-2} + \Sigma_2^{-2}}, \quad (79)$$

whereas at large  $\Sigma_1$ ,  $\Sigma_2$ , it logarithmically decreases:

$$V_\infty \simeq \frac{1}{2(\ln \Sigma_1 \Sigma_2 - \gamma_E - 1)}. \quad (80)$$

The dependence of  $V_\infty$  on both parameters  $\Sigma_1$  and  $\Sigma_2$  is shown in Fig. 6(a). Its maximum is achieved at  $\Sigma_1 = \Sigma_2 \approx 1$  [see Fig. 6(b)]. There, the function still does not exceed 0.7. Yet, in (58) it is multiplied by  $\Omega^{-2}$  with  $\Omega \gtrsim \pi$ , hence, actual visibility in the high- $\omega$  region is on the level of a few percent, demanding formidable measurement statistics.

For comparison, in Fig. 6(b) by dot-dashed curve we show the behavior of Eq. (78) after replacement of averaged radiation formfactors by non-averaged functions of averaged argument:

$$\langle F \rangle_\sigma \rightarrow F(\Sigma/2), \quad \langle G \rangle_\sigma(0) \rightarrow G(\Sigma, 0) = \frac{1}{2} - \frac{1}{2(1 + \Sigma^2)^2} \quad (81)$$

(LP-BD),

which we presume to correspond to Blankenbecler-Drell approximation. Function (81) intersects with the exact result at  $\Sigma \approx 2.5$ , and keeps close to it at greater  $\Sigma$ , but at  $\Sigma \approx 1$  the difference is rather large.

Fig. 6(c) compares predictions of Eq. (78) when averaging is performed with the Molière distribution, by Eqs. (73a), (38) (the blue solid curve for carbon, the red solid curve for gold), and with Gaussian distribution, Eqs. (62b) and (20) (black dashed curve). There is a distinct difference between the predictions around the maximum, which is achieved at  $l \approx 10^{-3} X_0$ , i.e.,  $\Sigma \approx 1$ . The sign of this difference tells that in the region of substantial photon energies, the account of fluctuations of scattering leads to a lowering of the interference effect in radiation, contrary to the situation with  $V_0$  in the previous section. That admits rather simple explanation: fluctuations always tend to suppress the radiation, but at  $\omega = 0$ , where the interference effect itself is suppressive, that worked towards increasing the effect, whereas in the large- $\omega$  region it just lowers both amplitudes  $\langle G \rangle_1(0)$  and  $\langle G \rangle_2(0)$  in the interference term.

## C. Spectrum oscillation shapes

For a generic case, integral (57) can only be evaluated numerically. But for limiting cases (53b) and (54), the integration is analytically manageable. For completeness, in the remainder of this section, we will collect formulae for the corresponding limiting spectral shapes, and compare them with results of [16], obtained for same limits, at  $\sigma_1 = \sigma_2$ .

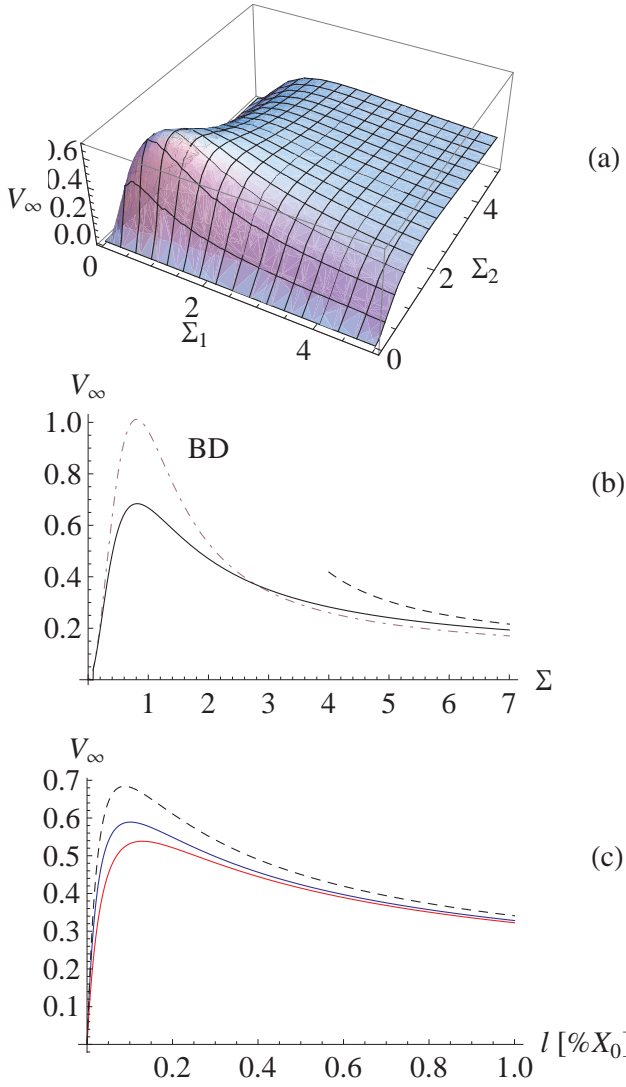


FIG. 6: Same as Fig. 5, for visibility of secondary minima and maxima, Eq. (78). The dashed curve in (b) obeys Eq. (80) for  $\Sigma_1 = \Sigma_2 = \Sigma$ .

### 1. Small-angle scattering in both plates

To begin with, consider the case when scattering angles in both of the foils are small. Inserting (63b) to (57), we get

$$\left\langle \frac{dI}{d\omega} \right\rangle_{\Sigma_{1,2} \ll 1} \simeq \left( \left\langle \frac{dI_1}{d\omega} \right\rangle + \left\langle \frac{dI_2}{d\omega} \right\rangle \right) \times \left( 1 + \frac{3}{5} \frac{1}{\Sigma_1^{-2} + \Sigma_2^{-2}} g_{\text{qq}}(\Omega) \right), \quad (82)$$

where

$$\left\langle \frac{dI_1}{d\omega} \right\rangle \simeq \frac{2e^2}{3\pi} \Sigma_1^2 \left( 1 - \frac{3}{10} \Sigma_1^2 \right), \quad (83)$$

and

$$g_{\text{qq}}(\Omega) = -20 \int_0^\infty \frac{d\Theta^2 \Theta^2}{(1 + \Theta^2)^6} \cos \Omega (1 + \Theta^2), \quad (84)$$

$$g_{\text{qq}}(0) = -1$$

is the quadrupole-quadrupole interference function. The latter function achieves its first (anti-LPM) maximum at  $\Omega \approx 2$  (see Fig. 7). According to Eqs. (82), (84), the visibility of spectral fringes is  $\sim \frac{3}{10} \Sigma_1^2$ .

It must be noted that our function (84) appears to differ from function  $\frac{10}{3} G(T)$  obtained in [16], Eq. (2.37). The comparison of those functions in Fig. 7 shows ample differences except in the limits  $\Omega = 0$  and  $\Omega \rightarrow \infty$ . We believe therefore that the corresponding result of [16] is in error.<sup>7</sup>

### 2. Radiation at double large-angle scattering

The next case to be considered is when scattering angles on each of the foils are  $\gg \gamma^{-1}$ . Inserting Eq. (64) to (57), obtains

$$\left\langle \frac{dI}{d\omega} \right\rangle_{\Sigma_{1,2} \gg 1} \simeq \frac{2e^2}{\pi} \left[ \ln \Sigma_1^2 + \ln \Sigma_2^2 - 2\gamma_E - 2 + g_{\text{II}}(\Sigma_1^{-2} + \Sigma_2^{-2}, \Omega) \right], \quad (85)$$

where

$$g_{\text{II}}(\xi, \Omega) = -\Re \left[ \int_0^\infty \frac{d\Theta^2 \Theta^2}{(1 + \Theta^2)^2} e^{-(1 + \Theta^2)(\xi + i\Omega)} \right]$$

$$= e^{-\xi} \cos \Omega - \Re \left[ (1 + \xi + i\Omega) E_1(\xi + i\Omega) \right], \quad (86)$$

with  $E_1(z) = \int_1^\infty dt \frac{e^{-zt}}{t}$  the exponential integral. Term  $\xi = \Sigma_1^{-2} + \Sigma_2^{-2}$  in the argument of  $E_1$  is negligible if  $\Omega \gg \Sigma_1^{-2} + \Sigma_2^{-2} \ll 1$ ; then our Eq. (85) reduces to Eq. (2.45) of [16]. This limiting function has an anti-LPM maximum at  $\Omega \approx 0.9$  (see Fig. 8), which agrees with the conclusions of Blankenbecler-Drell and Baier-Katkov that the maximum is achieved at  $\Omega \approx 1$ .<sup>8</sup> However, for small  $\Omega$ , term  $\xi$  in the argument of  $E_1$  is crucial. There,  $E_1(z) \simeq -\ln z - \gamma_E$ , wherewith

$$g_{\text{II}}(\xi, \Omega) \underset{\xi \ll 1}{\approx} \frac{1 + \xi}{2} \ln(\xi^2 + \Omega^2) + \gamma_E + 1 - \xi. \quad (87)$$

<sup>7</sup> In order to derive the corresponding result from equations (2.34), (2.36) of [16], one has to expand them up to  $b^{-2}$  (while contributions  $\sim b^{-1}$  from  $2dw_{br,1}^{(2)}/d\omega$  and  $dw_{br,3}^{(2)}/d\omega$  must cancel). We did not follow this procedure, wherefore we can not indicate the source of the error.

<sup>8</sup> However, we disagree with their interpretation of it as a unit-wavelength resonance. As was argued above, it is rather an inclined half-wavelength. Besides that, Baier and Katkov conducted their evaluation of the maximum for a specific value of the target thickness  $11 \mu\text{m}$ .

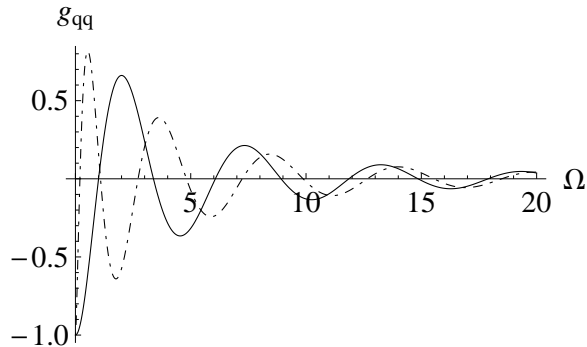


FIG. 7: Interference function for the case of double small-angle-scattering. Solid curve, Eq. (84) – close to the red curve of Fig. (4). Blue dot-dashed curve, Baier-Katkov's function  $\frac{10}{3}G(\Omega)$  [16].

Corrections proportional to  $\xi$ , especially in the prefactor of the logarithm in (87), can be important at moderately small  $\Sigma_1^{-2} + \Sigma_2^{-2}$ . Neglecting  $\Omega^2$  or  $\xi^2$  under the logarithm sign in (87), we arrive correspondingly at Eq. (2.42) or (2.43) of [16]. In Fig. 8 we compare the behavior of function (86) (solid curve), with that of approximation (87) (dotted curve), and of an approximation resulting when we put in Eq. (86)  $\Theta \rightarrow 0$  (dashed curve). The latter two approximations are seen to work in complementary regions.

### 3. Asymmetric case

Finally, we examine the case when one of the foils scatters weakly, whereas another one scatters the electrons through angles  $\gg \gamma^{-1}$ . Inserting the corresponding limiting forms (63b) and (64) to (57), we arrive at

$$\left\langle \frac{dI}{d\omega} \right\rangle_{\substack{\Sigma_1 \ll 1 \\ \Sigma_2 \gg 1}} \approx \frac{2e^2}{\pi} \left\{ \ln \Sigma_2^2 - \gamma_E - 1 + \frac{\Sigma_1^2}{3} [1 + g_{q1}(\Omega)] \right\}, \quad (88)$$

where

$$g_{q1}(\Omega) = -6 \int_0^\infty \frac{d\Theta^2 \Theta^2}{(1 + \Theta^2)^4} \cos \Omega(1 + \Theta^2), \quad (89)$$

$$g_{q1}(0) = -1.$$

This function has a maximum at  $\Omega \approx 1.6$ .

Notably, there is no logarithmic dependence in the interference term, and its amplitude does not depend on  $\Sigma_2$ , which corresponds to strict saturation of radiation. Correspondingly, the visibility in this case is  $\sim \frac{\Sigma_1^2}{\ln \Sigma_2^2}$ , i.e., even lower than for the case of double small-angle scattering.

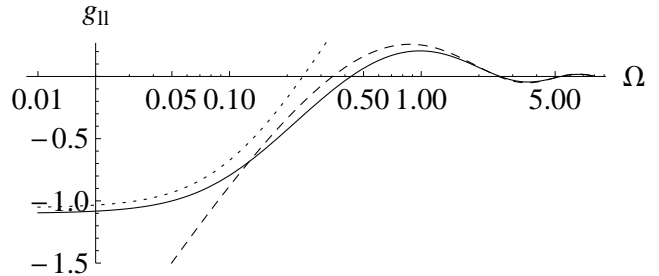


FIG. 8: Interference function for the case of double large-angle-scattering. Solid curve, Eq. (86) – close to the blue curve of Fig. 4. Dashed curve,  $g_{11}(0, \Omega)$ . Dotted curve, asymptotics (87).

## VI. ACCOUNT FOR FOIL THICKNESS(ES)

Hitherto we presumed negligible thicknesses of both targets, but at a sufficiently large  $\omega$ , finite target thickness must inevitably show up. Indeed, when  $l_f$  decreases down to the value of  $l$ , the target geometry gets resolved. Thereat, the radiation spectrum must additionally rise from the doubled but logarithmically saturated values to the completely saturation-free Bethe-Heitler value.

In principle, our framework requires only minor modification to reflect the mentioned rise: It suffices to multiply the radiation spectrum computed above by the plate formfactor, which smoothly interpolates between unity at  $\omega \lesssim \frac{2\gamma^2}{t_{21}}$  and Migdal's function  $\Phi_M$  at  $\omega \gg \frac{2\gamma^2}{t_{21}}$  (specifically,  $\omega \gtrsim e^2 \frac{\gamma^2 X_0}{l^2}$ ). The implementation of such an interpolation, however, is beyond our scope in the present paper.

## VII. COMPARISON WITH EXPERIMENT

The best way to test our equations is to confront them with experimental data. Measurements of bremsstrahlung spectra from 178 GeV electrons on a sequence of plates were performed in [18, 19] with two equal 26  $\mu\text{m}$  thick golden foils ( $X_0^{\text{Au}} = 3.4 \text{ mm}$ ) separated by a gap of variable width. The scattering strength parameter for one such a foil, according to Eq. (44), estimates as  $\gamma\sigma \approx 2.7$ , so the scattering angles there were rather large.

In Fig. 9 we compare predictions of our Eq. (57) and Eq. (71) with the experiment [19], letting  $t_{21}$  be equal to the distance between plate centres,  $l_g + l$ . The agreement may be regarded as fair. Some possible experimental inaccuracies at  $\omega \lesssim 50 \text{ MeV}$  were discussed in [18], but they do not seem to cause large deviations.

Since our Gaussian and Molière averaging procedures give numerically close results, and on the other hand, it was found in Sec. III that our prescriptions for scattering parameters are close to those of Baier-Katkov and Zakharov, we expect that Baier-Katkov's and Zakharov's

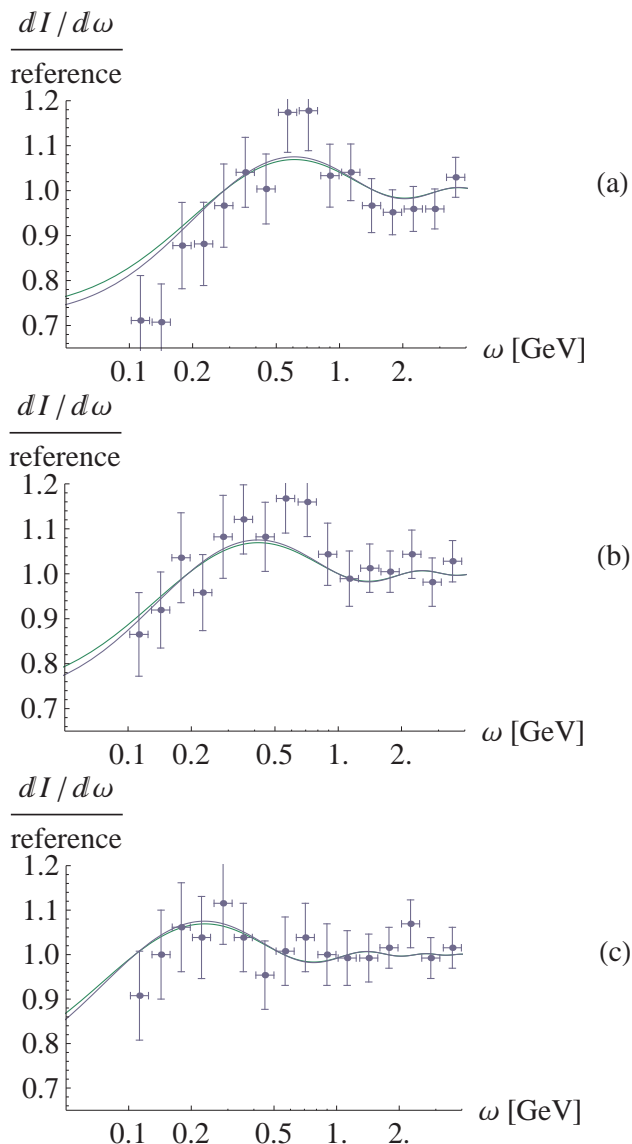


FIG. 9: Shapes of spectral oscillations for conditions of experiment [19] ( $l_1 = l_2 = 26\mu\text{m}$ ). (a)  $t_{21} = 26 + 60\mu\text{m}$ ; (b)  $t_{21} = 26 + 100\mu\text{m}$ ; (c)  $t_{21} = 26 + 200\mu\text{m}$ . Dark blue curves, Gaussian averaging, with  $\Sigma$  calculated by Eq. (44). Green curves, Molière averaging for gold.

predictions for the radiation spectrum must be in agreement with the experiment [19], too, even though the qualitative inferences based on the Baier-Katkov theory seem to disagree with it.

As for comparison of experimental results with predictions of Blankenbecler, recalling our results of Sec. V, it should be noticed that the use of plates with scattering strength  $\gamma\sigma \approx 2.7$  closely corresponds to the point of intersection of visibilities in BD approximation with exact ones [see Fig. 6(b)]. Therefore, Blankenbecler's predictions may agree with particular experiment [19] rather nicely, too. Basic agreement of experimental results with [14] (and disagreement with [15]) was actually reported

in [19]. However, for foils several times thinner than currently used (or made of a lighter material), we predict a growing inaccuracy of Blankenbecler-Drell predictions. At the same time, for weaker scattering foils, the visibility of *secondary* spectral minima and maxima can yet increase by about a factor of 2 [see Figs. 6(b),(c)].

### VIII. BREMSSTRAHLUNG ON RANDOMLY LOCATED PLATES

Having dwelt enough on the case of bremsstrahlung on two targets separated by a fixed distance, it would be instructive also to generalize it so that it could be compared with the conventional case of bremsstrahlung in an extended random medium. Of course, presently we possess equations for radiation only at two scatterings, but arguably, the greatest contribution to the interference must come from nearest scatterings. Therefore, we can exploit previous formulae, if  $t_{21}$  is regarded as a random variable distributed within some range  $\sim \tau$ . Rather realistically, it can be modeled by an exponential  $e^{-t_{21}/\tau}$ , corresponding to the probability of avoiding an encounter with the next atom in a uniform gas with the mean interatomic distance  $\tau$ . To preserve the anti-LPM effect, though, we must prevent  $t_{21}$  from tending to zero, as was pointed out in Sec. II. For simplicity, we shall assume the shape of the anticorrelation to be described also by an exponential, but shorter-range one, thus choosing the distribution function

$$\frac{dw}{dt_{21}} = \frac{1}{\tau - a} \left( e^{-t_{21}/\tau} - e^{-t_{21}/a} \right). \quad (90)$$

Parameter  $a < \tau$  provides the 'repulsion' distance between the scatterers. Weighting Eq. (57) with (90), we get

$$\begin{aligned} \left\langle \frac{dI}{d\omega} \right\rangle_{t_{21}} &= \frac{2e^2}{\pi} \left\{ \langle F \rangle_1 + \langle F \rangle_2 \right. \\ &+ \frac{4}{\tau - a} \int_0^\infty d\Theta^2 \Theta^2 \langle G \rangle_1 \langle G \rangle_2 \\ &\times \left[ -\frac{\tau}{1 + \left(\frac{\omega\tau}{2\gamma^2}\right)^2 (1 + \Theta^2)^2} + \frac{a}{1 + \left(\frac{\omega a}{2\gamma^2}\right)^2 (1 + \Theta^2)^2} \right] \left. \right\} \quad (91) \end{aligned}$$

The  $\omega$ -depending factor in the integrand is now a difference of Lorentzians (bell-shaped functions of definite sign) having different heights and widths determined by  $\tau$  or  $a$ , but equal areas. The first term in the brackets is negative, and can be associated with LPM-like uniform suppression, whereas the second term is positive, representing the anti-LPM enhancement, which is now strictly positive and non-oscillatory. The shapes of radiation-angle-integral spectra are illustrated in Fig. 10 for same values of  $\Sigma$  as in Fig. 4, and (for the sake of illustration) a moderately large ratio  $\tau/a = 3$ . It may be observed that with the increase of  $\Sigma$ , the shape of LPM-like suppression sharpens towards  $\omega \rightarrow 0$ , although it does not



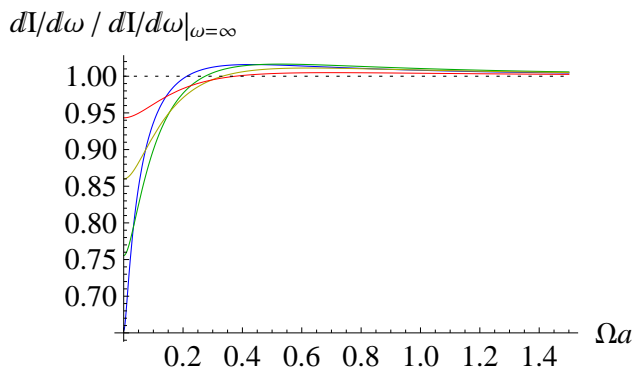


FIG. 10: Spectra of bremsstrahlung on two plates with a randomized distance between them, Eq. (91), for  $\tau = 3a$  and same parameter values for scattering strengths as in Fig. 4.

tend to the thick-target dependence  $\sim \sqrt{\omega}$ . Obviously, to get the  $\sqrt{\omega}$  behavior, more than two scatterings need to be involved.

Finally, we note that in atomic matter, scales  $\tau$  and  $a$  should vastly differ. To estimate  $\tau$ , it may suffice to note that according to Migdal's calculation, typical  $\omega$  at which LPM effect develops are  $\sim \frac{\gamma^2}{l_{\text{scat}}}$ , where

$$l_{\text{scat}} = \frac{l}{\Sigma^2(l)} \sim \frac{\alpha}{2\pi} X_0 \sim \frac{1}{8\pi Z^2 \alpha^4} a_{\text{B}}$$

is the range at which the angle of multiple scattering becomes comparable with the radiation angle  $\gamma^{-1}$ . Hence,  $\tau \sim l_{\text{scat}}$ , and owing to the presence of factor  $Z^{-2}\alpha^{-4}$ , this range is at least by 4 orders of magnitude greater than typical interatomic distance (a few units of  $a_{\text{B}}$ ), which must constitute the scale for  $a$ . Therefore, anti-LPM enhancement in atomic matter must be virtually invisible indeed, reconciling its principal existence with the conventional theories of the LPM effect. Put differently,  $|t_2 - t_1|$  can be effectively sent to zero, justifying the formal use of the  $\delta$ -correlated model of multiple scattering employed by Migdal [3].

## IX. SUMMARY

In course of our study, we arrived at the following conclusions:

- For scattering foils with macroscopic and fixed separation, the LPM-like suppression of bremsstrahlung at lowest  $\omega$  is accompanied by an adjacent enhancement, which can be called the anti-LPM effect. The latter effect may be associated with an inclined-half-wavelength resonance [see Eq. (60)], but not with the unit wavelength resonance, as was previously suggested in [14]. In classical electrodynamics, LPM and anti-LPM effects are predicted to have equal strength, in the sense that their  $\omega$ -integrated effect is zero (see the

end of Sec. II). However, in a random and weakly scattering media, like the ordinary atomic matter, the anti-LPM enhancement is expected to smear over a broad spectral interval, and thus become faint.

- The shape of the anti-LPM maximum depends on the strength of the scattering in each plate (see Fig. 4). It assumes universal forms for limits of strong or weak scattering: For small scattering angles in both plates, the shape of the oscillatory pattern in the spectrum is described by Eq. (84). For large scattering angles in both plates, it is described by function (86) (unifying different limiting cases described in [16]). For the mixed case when one plate scatters strongly, and another one weakly, the spectrum shape obeys Eq. (89), where the dependence of the interference term on  $\Sigma$  strictly saturates.
- At asymptotically large  $\omega$ , the dominant contribution to the interference term stems from photon emission angles close to  $\mathbf{v}_2$ , such that  $|\mathbf{n} - \mathbf{v}_2| < \sqrt{\frac{2}{\omega t_{21}}} < \frac{1}{\gamma}$ . Therewith, the interference term scales as  $\propto \frac{\cos \Omega}{\Omega^2}$ , with the coefficient proportional to the product of  $G$ -amplitudes of radiation emitted strictly parallel to  $\mathbf{v}_2$  [see Eq. (58)]. Granted this universality, the locations of *secondary* maxima and minima are virtually independent of the scattering strength in the plates.

We have also established that if the rms scattering angle is calculated with a proper account of Coulomb corrections, the predictions of Gaussian averaging are pretty close to those of the more precise Molière averaging, and practically comply with the results of Zakharov [7], and Baier and Katkov [16]. For 2 scattering plates, the equation for Molière averaging is basically as simple as that for Gaussian averaging.

Finally, we note that satisfactory agreement of predictions of classical electrodynamics with experiment was found. For future experiment planning, it may be useful to refer to visibilities of the interference minima and maxima at low and at large  $\omega$ , computed in Sec. V (Figs. 5 and 6).

It may be added that prospects of observing anti-LPM effect in radiation may be not restricted to artificial assemblies of plates, provided one finds a case when  $l_{\text{scat}} \sim a$ , i.e., every constituent of the matter can scatter the radiating projectile relativistically. Conditions for such a situation may be sought, for instance, in nuclear matter.

## Acknowledgements

This work was supported in part by UFFR Project No. 58/17.

### Appendix A: Derivation of empirical formula (44) from Molière distribution

To clarify the success of the Gaussian approximation in conjunction with interpolation (44) for the rms scattering angle, consider the large- $\chi_c$  limit of Eq. (38):

$$\begin{aligned}
\langle F \rangle_M &= 2 \int_0^\infty d\rho \rho K_1^2(\rho) \left\{ 1 - e^{-\frac{\chi_c^2}{\chi_1^2} [1 - \rho \gamma \chi_1 K_1(\rho \gamma \chi_1)]} \right\} \\
&\simeq 2 \int_0^{\rho_0} \frac{d\rho}{\rho} \left\{ 1 - e^{-\frac{1}{2} \rho^2 \gamma^2 \chi_c^2 \left( \ln \frac{2}{\gamma \chi_1 \rho} + \frac{1}{2} - \gamma_E \right)} \right\} \\
&\quad + 2 \int_{\rho_0}^\infty d\rho \rho K_1^2(\rho) \\
&\simeq \int_0^{\rho_0^2} \frac{d\rho^2}{\rho^2} \left\{ 1 - e^{-\frac{1}{4} \rho^2 \gamma^2 \chi_c^2 \left[ \ln \left( \frac{\chi_c^2}{\chi_1^2} \ln \frac{\chi_c^2}{\chi_1^2} \right) + 1 - 2\gamma_E \right]} \right\} \\
&\quad + 2 \left( \ln \frac{2}{\rho_0} - \frac{1}{2} - \gamma_E \right) \\
&\simeq \ln \left\{ \gamma^2 \chi_c^2 \left[ \ln \left( \frac{\chi_c^2}{\chi_1^2} \ln \frac{\chi_c^2}{\chi_1^2} \right) + 1 - 2\gamma_E \right] \right\} - 1 - \gamma_E.
\end{aligned} \tag{A1}$$

Comparing it with Eq. (21), we establish the correspondence

$$\Sigma^2 = \gamma^2 \chi_c^2 \left[ \ln \left( \frac{\chi_c^2}{\chi_1^2} \ln \frac{\chi_c^2}{\chi_1^2} \right) + 1 - 2\gamma_E \right]. \tag{A2}$$

If we neglect here  $1 - 2\gamma_E \approx -0.15$ , and substitute  $\frac{\chi_c^2}{\chi_1^2}$  from Eq. (42), it casts as

$$\begin{aligned}
\Sigma^2 &= \frac{\pi}{e^2} \left( \ln \frac{1}{\gamma^2 \chi_1^2} + \frac{7}{6} \right) \frac{2l}{X_0} \\
&\quad \times \left[ \ln \frac{1}{\gamma^2 \chi_1^2} + \ln \frac{\pi}{e^2} + \ln \frac{\ln \frac{\chi_c^2}{\chi_1^2}}{\ln \frac{1}{\gamma \chi_1} + \frac{7}{12}} + \ln \frac{l}{X_0} \right].
\end{aligned} \tag{A3}$$

Next, one can put  $\ln \frac{\pi}{e^2} \approx 6$ ,  $\ln \frac{1}{\gamma^2 \chi_1^2} \approx 8 \pm 2$ ,  $\ln \frac{\ln \frac{\chi_c^2}{\chi_1^2}}{\ln \frac{1}{\gamma \chi_1} + \frac{7}{12}} \sim 1$ , and  $\ln \frac{l}{X_0}$  can vary from  $-7$  (if  $l = 10^{-3} X_0$ ) to  $-2$  (if  $l = 10^{-1} X_0$ ). As a result,  $\Sigma$  can be approximated by

$$\Sigma \approx \frac{\mu}{m_e} \sqrt{\frac{2l}{X_0}} \sqrt{1 + 2c \ln \frac{l}{X_0}} \approx \frac{\mu}{m_e} \sqrt{\frac{2l}{X_0}} \left( 1 + c \ln \frac{l}{X_0} \right), \tag{A4}$$

with  $\mu \approx \sqrt{\frac{\pi}{e^2} \frac{8+6+1}{8+7/6}} m_e \approx 13.6$  MeV, and  $c \approx \frac{1}{2(8+6+1)} \approx 0.033$ . Those numbers comply with the coefficients in Eq. (44), which we have thereby derived ab initio. Parameter  $\mu$  can also be compared with Rossi's  $E_s = \sqrt{\frac{4\pi}{e^2}} m_e = 21.2$  MeV. Product  $\mu \left( 1 + c \ln \frac{l}{X_0} \right)$  becomes twice smaller than  $E_s$  at  $l \sim 10^{-3} X_0$ , which then exactly corresponds to approximation (25). In general case, of course, it is more reliable to use formula with an explicit  $\ln l/X_0$  dependence, like (44).

- 
- [1] M.L. Ter-Mikayelyan. *High Energy Electromagnetic Processes in Condensed Media*. New York: Wiley, 1972; V.N. Baier, V.M. Katkov, V.S. Fadin, *Radiation from Relativistic Electrons* (in Russian) Moscow: Atomizdat, 1973; A.I. Akhiezer, N.F. Shul'ga. *High Energy Electrodynamics in Matter*. Amsterdam: Gordon & Breach, 1996.
- [2] L.D. Landau and I.Ya. Pomeranchuk, Dokl. Akad. Nauk. SSSR **92** (1953) 535; *ibid.*, **92** (1953) 735.
- [3] A.B. Migdal, Phys. Rev. **103** (1956) 1811.
- [4] F.F. Ternovskii, Zh. Eksp. Teor. Fiz. **39** (1960) 171 [Sov. Phys. JETP **12** (1961) 123].
- [5] V.E. Pafomov, Zh. Eksp. Teor. Fiz. **49** (1965) 1222 [Sov. Phys. JETP **22** (1966) 848].
- [6] R. Blankenbecler and S.D. Drell, Phys. Rev. D **53** (1996) 6265.
- [7] B.G. Zakharov, Pis'ma **64** (1996) 737 [JETP Lett. **64** (1996) 781]; Yad. Fiz. **61** (1998) 924 [Phys. At. Nucl. **62** (1998) 1008].
- [8] V.N. Baier and V.M. Katkov, Phys. Rev. D **57** (1998) 3146.
- [9] N.F. Shul'ga and S.P. Fomin, JETP Lett. **27** (1978) 117; Zh. Eksp. Teor. Fiz. **113** (1998) 58 [JETP **86** (1998) 32]; NIM B **145** (1998) 73.
- [10] P. Anthony *et al.*, Phys. Rev. D **56** (1997) 1373; H.D. Hansen *et al.*, Phys. Rev. D **69** (2004) 032001.
- [11] S. Klein, Rev. Mod. Phys. **71** (1999) 1501.
- [12] A.I. Akhiezer, N.F. Shul'ga and S.P. Fomin, Phys. Reviews **22** (2004) 1.
- [13] V.N. Baier and V.M. Katkov, Phys. Rep. **409** (2005) 261.
- [14] R. Blankenbecler, Phys. Rev. D **55** (1997) 190; Preprint SLAC-PUB-96-7156, Stanford, 1996.
- [15] R. Blankenbecler, Phys. Rev. D **55** (1997) 2441.
- [16] V.N. Baier and V.M. Katkov, Phys. Rev. D **60** (1999) 076001.
- [17] H.D. Thomsen *et al.*, Phys. Rev. D **81** (2010) 052003.
- [18] K.K. Andersen *et al.*, Phys. Rev. Lett. **108** (2012) 071802.
- [19] K.K. Andersen *et al.*, Phys. Lett. B **732** (2014) 309.
- [20] G. Diambrini Palazzi, Rev. Mod. Phys. **40** (1968) 611.
- [21] J.D. Jackson. *Classical Electrodynamics*, 3rd ed., New York: Wiley, 1998; L.D. Landau, E.M. Lifshitz. *The Classical Theory of Fields*, Oxford: Elsevier, 1975.
- [22] J.S. Bell, Nucl. Phys. B **8** (1958) 613.
- [23] V.B. Berestetskii, E.M. Lifshitz, L.P. Pitaevskii, *Quantum Electrodynamics*. Oxford: Pergamon-Press, 1982.
- [24] G. Moliere, Z. Naturforsch. A **2** (1947) 133; **3** (1948) 78.

- H.A. Bethe, Phys. Rev. **89** (1953) 1256.
- [25] J.D. Bjorken, J.B. Kogut, and D.E. Soper, Phys. Rev. D **3** (1971) 1382.
- [26] V.L. Highland, NIM **129** (1975) 497.
- [27] G.R. Lynch and O.I. Dahl, NIM B **58** (1991) 6.
- [28] J. Beringer *et al.* (Particle Data Group), Phys. Rev. D **86** (2012) 010001.
- [29] Y.-S. Tsai, Rev. Mod. Phys. **46** (1974) 815.
- [30] M. Abramowitz, I.A. Stegun. *Handbook of Mathematical Functions*. New York: Dover, 1972.
- [31] R.J. Glauber, Phys. Rev. **100** (1955) 242.
- [32] V.M. Galitsky and I.I. Gurevich, Nuov. Cim. **32** (1964) 396.